Comparison of Pre-stack Noise Suppression Techniques for AVO Analysis

---

A Thesis Presented to
the Faculty of the Department of Earth
and Atmospheric Sciences
University of Houston

In Partial Fulfillment
of the Requirement for the Degree
Master of Science

By

Dong Liu

December, 2012

Comparison of Pre-stack Noise Suppression Techniques for AVO Analysis

Dong Liu

APPROVED:

Dr. John P. Castagna, Chairman

Dr. Evgeny Chesnokov

Dr. Oleg Portniaguine

Dean, College of Natural Sciences and Mathematics

ACKNOWLEDGMENTS

I wish to thank Dr. John Castagna for all his advice during my research and classes at the University of Houston. Special thanks to my committee members Dr. Oleg Portniaguine and Dr. Evgeny Chesnokov for their guidance and suggestions on this work.

My deepest gratitude goes to Lumina Geophysical and Dataseismic Geophysical Services for providing the data and financial support during this study. Especial thanks to Alejandro Juranovic, Maria Virginia Mason, Carlos Moreno, and Gabriel Gil; their comments and suggestions were very important during this work.

I would like to thank the entire Department of Earth and Atmospheric Sciences at the University of Houston for all its help during my academic period; I especially want to thank Sylvia Marshall, Erika Brown, and Laura Bell for all their help, advice, suggestions, and helpful tips.

Thanks to all my friends at UH, especially: Lorenzo Izarra, Juan Berrizbeitia, Gisela Porfiri, Vanessa Lobo, Jose Antonio Sierra, Luanxiao Zhao, Lun Li, Arnold Oyem, and Umberto Barbato. With you guys I have shared very enjoyable moment.

My eternal gratitude goes to my Dad and Mom. You have always supported me and have had confidence that I would achieve my dreams.

Last but not least, to my wife Yuanfei: you have always been there with me; and your support is an important part of all the things that I do in my life.

Comparison of Pre-stack Noise Suppression Techniques for AVO Analysis

---

An Abstract of a Thesis
Presented to
the Faculty of the Department of Earth
and Atmospheric Sciences
University of Houston

In Partial Fulfillment
of the Requirement for the Degree
Master of Science

By

Dong Liu

December, 2012

ABSTRACT

Synthetic study has proved that post-stack Structural Filter (SF) applied to Common Offset (CO) gathers with pilot-stack showed better performance over FK Dip Filter and FX Decon with regard to fault preservation, noise suppression, and amplitude preservation; in Common Midpoint (CMP) domain, Radon Filter and Structural Filter suppressed random noise, spikes, and multiples with high efficiency. SF with padded intercept was superior to Radon Filter, because it preserved the reflection amplitude with offset variation. The application of Structural Filter in Stratton Field data showed that the best workflow was the cascaded process. The cascaded SF has been demonstrated to be superior over conventional noise suppression methods, because it preserved relative amplitude, removed random noise, flattened seismic reflectors, and enhanced faults and fractures. In addition, by applying Structural Filter to pre-stack time migrated gathers, the improved velocity produced better stack sections for further structure identification and interpretation. Using the conditioned CRP gathers in AVO analysis, it improved intercept and gradient sections and AVO cross-plot. The intercept and gradient sections showed negative intercept and gradient for top reservoir sand, indicating a class III AVO response. AVO cross-plots showed that SF defined a clustered background trend which allowed us to differentiate deviations associated with top and base of the reservoir. Both synthetic study and real data application proved that SF is an AVO compliant noise suppression technique, and is a great tool for AVO data conditioning. The application of Structural Filter in Stratton Field data for AVO analysis may potentially help to find new prospect for exploitation and production in the Gulf Coast Basin.

CONTENTS

Chapter 1

Introduction

AVO analysis demands high-quality seismic data. Special amplitude preserving processing techniques are needed since AVO analysis is performed on pre-stack gathers. In pre-stack AVO analysis, CDP stacking, the most powerful noise suppression tool in the processing of seismic reflection data, is only available in the form of limited range (partial) stacks. Therefore, pre-stack noise suppression techniques are particularly important (Castagna, 2001). Because of the important role of pre-stack noise suppression techniques in AVO analysis, they are the main focus of this study.

There are many noise suppression methods in the pre-stack domain, and they can be classified based on what kind of noise that exists in the seismic data they deal with. In this thesis, four pre-stack noise suppression techniques will be studied. Structural Filter as a new approach to pre-stack noise suppression is compared to three conventional methods: Radon Filter, FK Dip Filter, and FX Decon.

The main objectives of this study are: evaluate Structural Filter in synthetic and real seismic data; compare the results with other conventional methods; and verify that the use of Structural Filter in pre-stack seismic data enhances Signal-to-Noise Ratio (SNR), removes random noise, preserves relative seismic amplitude, flattens seismic reflectors, and enhances stratigraphic features such as faults and fractures.

The first part of this research is to evaluate and compare the four pre-stack noise suppression techniques in synthetic seismic data, and determine the advantages and disadvantages of Structural Filter over Radon Filter, FK Dip Filter, and FX Decon.

After the synthetic study, Structural Filter is applied to a 3D seismic data set (92-BEG 3D seismic survey) from Stratton Field, located at Nueces County, Texas. The study area is showed in Figure 1.

The Stratton Field 3D seismic data covers a 2 mi^2 (5.2 km^2) area and was acquired by Bureau of Economic Geology (BEG) in 1992. The data contains a large number of wells that were drilled and used in making geologic analysis of the Frio reservoirs.

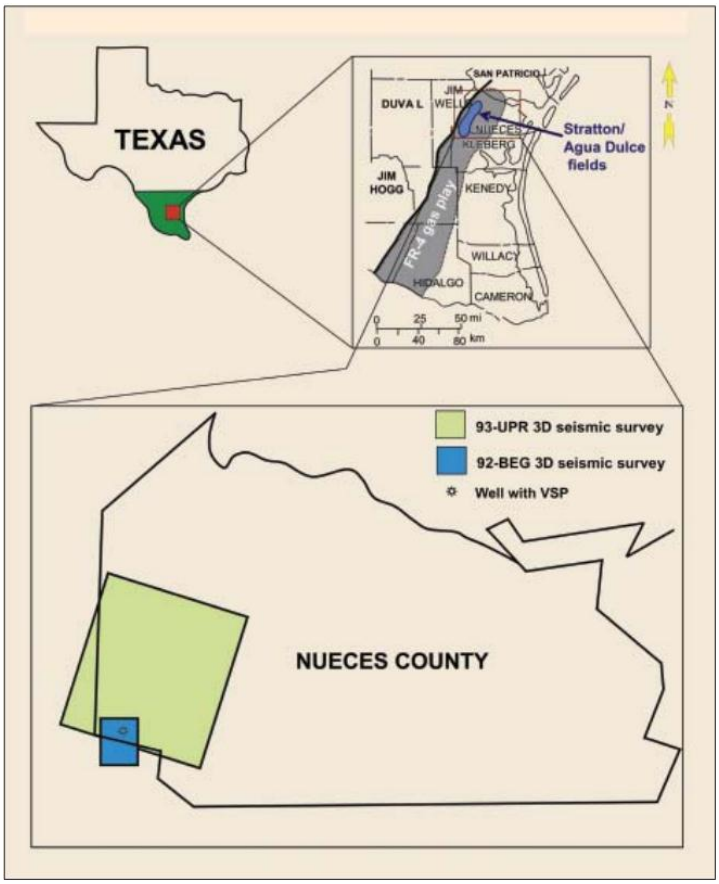

Figure 1. The study area is located at the southwest part of Nueces County, Texas. Modified from El-Mowafy and Marfurt, 2008.

The target for this study is the basal part of the middle Frio Formation represented by the F11 horizons (Figure 2). The Frio Formation, as a major hydrocarbon producer in the Texas Gulf Coast, consists of multiple vertically stacked reservoir sequences. The structural setting of the middle Frio in the study area is predominantly growth faults and associated rollover anticlines (El-Mowafy and Marfurt, 2008).

By applying Structural Filter in Stratton Field 3D seismic data, improvement in Signal-to-Noise Ratio (SNR), velocity analysis, seismic reflectors continuity, and preservation of seismic amplitude is to be expected. Most importantly, it is to be expected that preconditioning seismic data using Structural Filter will contribute to a better result in AVO analysis.

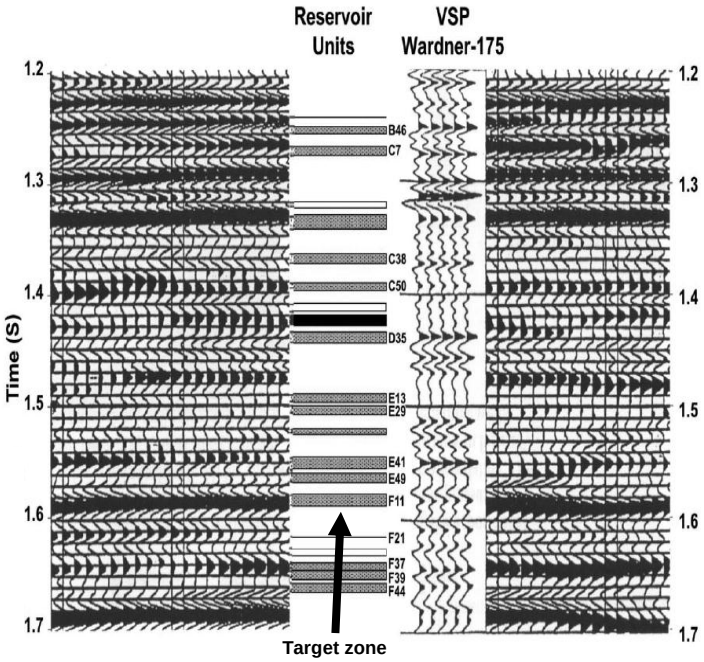

Figure 2. VSP data from well Wardner 175. Horizon of interest is F11 at ~1.58s. (Modified from El-Mowafy and Marfurt, 2008).

This thesis has been divided into six chapters. Chapter 1 describes the main objectives of this study, general concepts regarding the pre-stack noise suppression

techniques used in this study, and presents the study area location and major characteristics of the Frio Formation, Stratton Field.

In Chapter 2, the geology related to Gulf Coast Basin is presented; major structural and tectonic elements, stratigraphic features, and the hydrocarbon potential are described.

Chapter 3 presents the theory behind Structural Filter, Radon Filter, FK Dip Filter, and FX Decon, describing general concepts of these methods, characteristics, advantages, and disadvantages.

In Chapter 4, a description of the methodology used for this thesis is presented, including data description, synthetic data generation, and workflow.

Chapter 5 presents the results and discussion. The first part shows how Structural Filter is performed in synthetic data evaluation; the second part illustrates the results of the application of Structural Filter in Stratton Field data, and compares of the results with Radon Filter, FK Dip Filter, and FX Decon.

This thesis ends in Chapter 6, with the major conclusions derived from the analysis of the results presented in Chapter 5.

Chapter 2

Geological Setting

This chapter will describe the characteristics of the geological setting that constitute the Stratton Field Gulf Coast Basin. First, a brief description of regional structural elements and the tectonic configuration is presented; second, a detailed picture of the stratigraphy is given by describing the Vicksburg and Frio Formations; and finally, the explanation about how and why the target of this study has been chosen is presented.

Regional Structural and Stratigraphic Setting

According to Levey (Levey et al., 1994), The Oligocene Frio Formation is one of the major progradational offlapping stratigraphic units in the northwest Gulf Coast Basin. Figure 3 shows a schematic of the depositional sequences present in the Texas Gulf Coast Basin, where the Frio Formation is observed.

The Frio Formation is a sediment supply dominated depositional sequence characterized by rapid deposition and high subsidence rates (Galloway et al., 1982; Morton and Galloway, 1991). The major sediment source of the Frio Formation is supplied by the Rio Grande Embayment.

As Levey stated, "The Oligocene Frio Formation of Texas is volumetrically the largest gas productive interval of 10 major depositional stratigraphic packages in the Cenozoic Gulf Coast Basin"

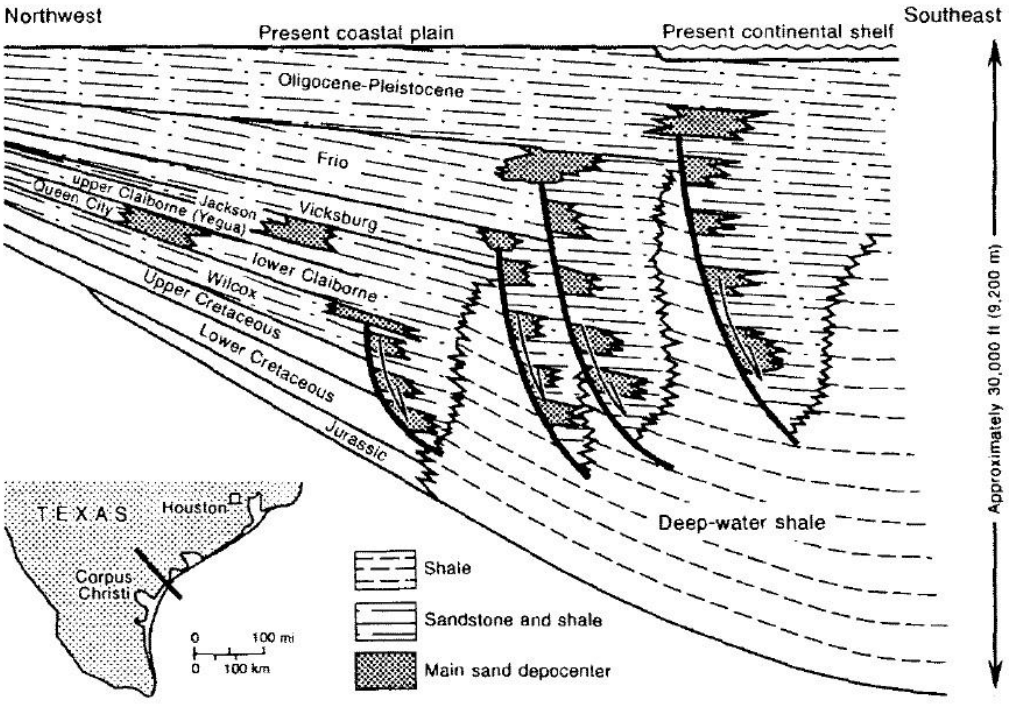

Figure 3. Depositional dip-oriented cross section through the Texas Gulf Coast Basin illustrating the relative position of major sand depocenters (After Bebout et al., 1982).

Figure 4 shows the relative rank of volume of gas produced in a typical Stratigraphic column of the onshore Texas Gulf Coast Basin.

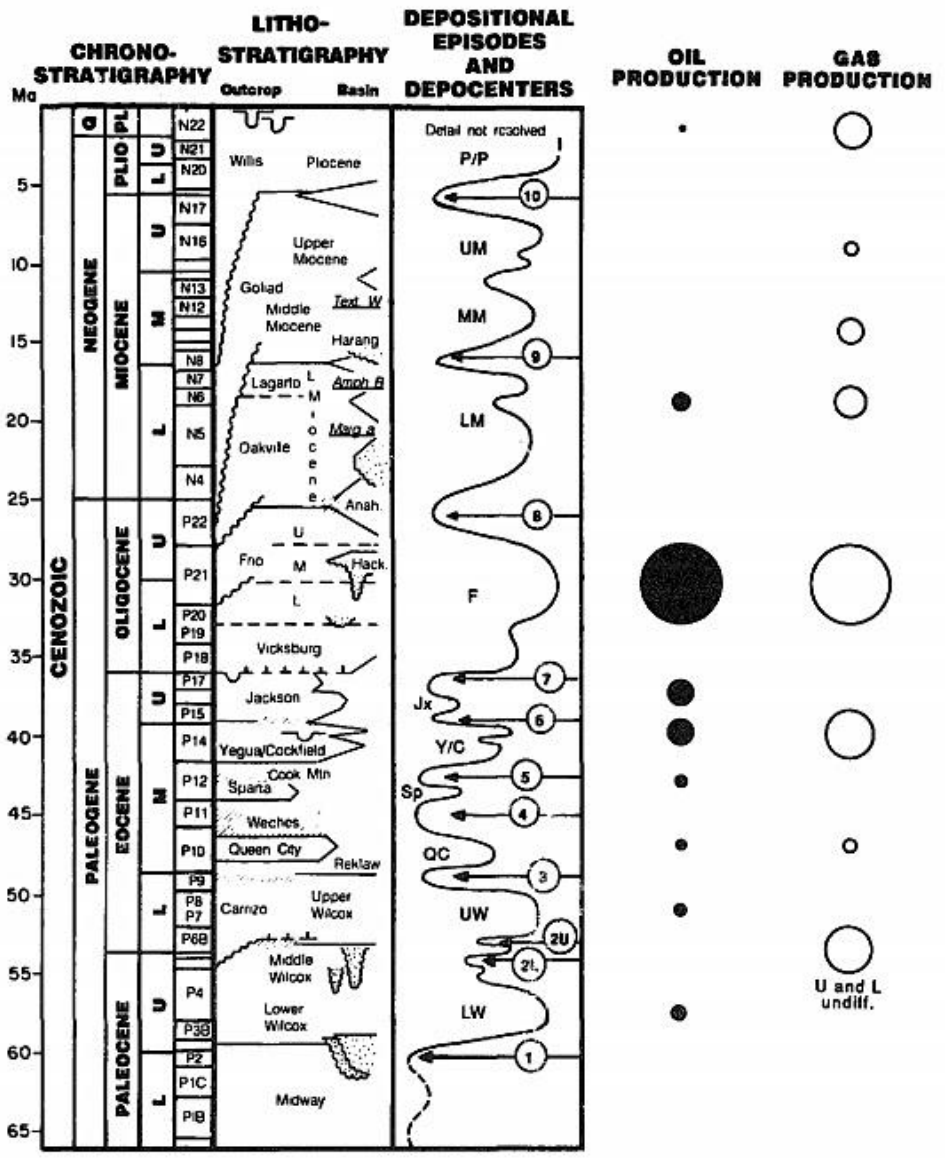

Figure 4. Stratigraphic distribution of oil and gas production of the onshore Gulf Coast Basin. (Modified From Galloway et al., 1983.)

As Levey concluded, "The Oligocene Frio Formation is the largest gas productive interval in the Gulf Coast Basin". Within the Frio Formation, the most productive middle Frio interval was deposited during the Catahoula-Frio depositional episode described by Galloway (Galloway, 1977).

Structural and Stratigraphic Setting of Stratton Field

The 3-D seismic and well log data set from Stratton Field belong to the 92-BEG 3D seismic survey, located at the southwest part of Nueces County, Texas (Figure 1 - Chapter 1). The structural element of the Frio and Vicksburg reservoirs in Stratton Field is illustrated by a structural dip-oriented seismic line across the target of this study (Figure 5). Gas reservoirs in the Vicksburg and lower Frio Formations are affected by a series of normal faults and structural rotation above the Vicksburg decollement surface (Levey et al., 1994). The relatively undeformed and flat-lying middle and upper Frio Formation is structurally much simpler than the underlying Vicksburg and lower Frio. Analysis of both well log correlations and 2-D reflection seismic data indicates that only a few faults extend upward into the middle Frio (Hardage et al., 1996).

As a major hydrocarbon producer in the Texas Gulf Coast, Stratton Feld in south Texas was discovered in 1922. It had cumulative gas production more than 1.5 TCF untill 1994 (Levey et al., 1994). The field produces gas from the Oligocene-age Frio Formation, as described above a thick, fluvially deposited sandstone-shale sequence that is a prolific producer along a regional depositional trend. This trend was a result of major progradation during an eight million year period (Galloway et al., 1982).

The main hydrocarbon trapping mechanisms in the Frio Formation are controlled both by structural and stratigraphic factors, including faulted anticlinal closure, facies change, and reservoir pinch-out (Kosters et al., 1989).

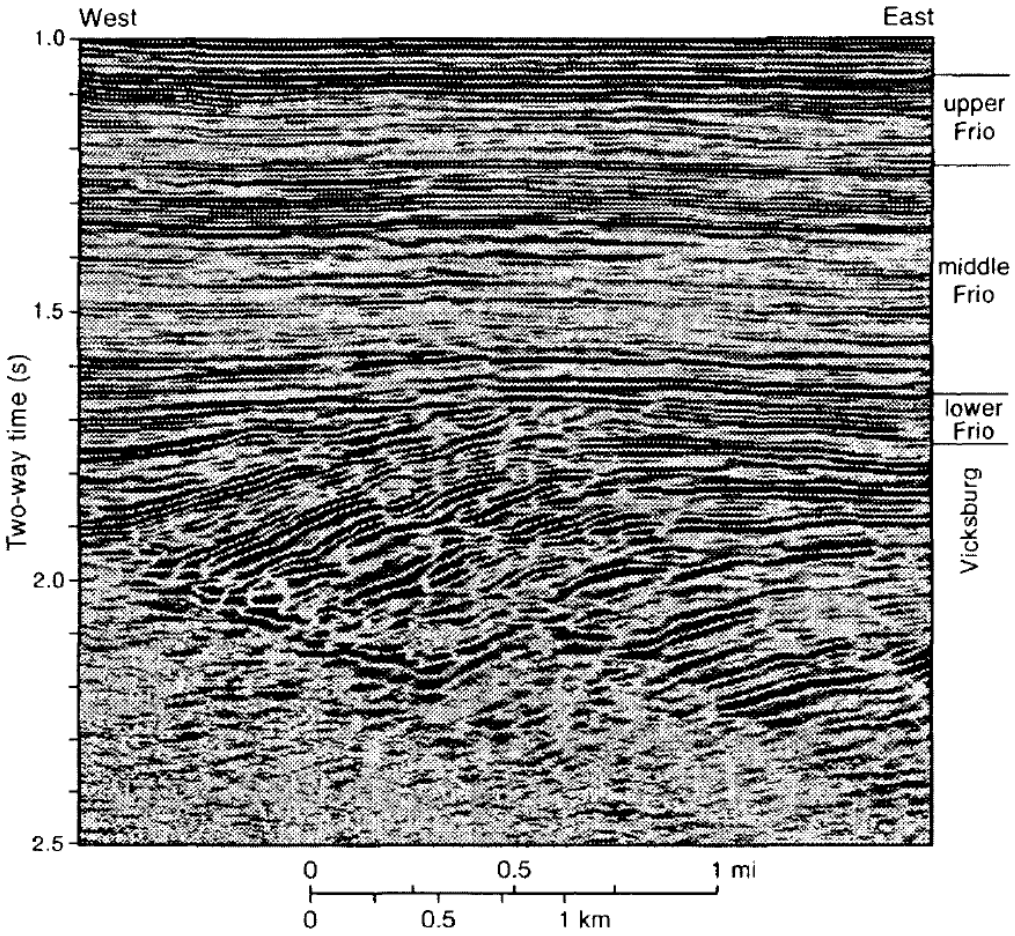

Figure 5. Subregional dip-oriented reflection seismic line through Stratton Field showing faulting blocks in the lower Frio and Vicksburg Formations, which contrasts sharply with the lack of faulting in the middle and upper Frio Formation.

Within the Frio Formation, the most productive middle Frio interval is aggradational in nature. Aggradation rates alternated over time; lateral and vertical stacked fluvial-splay channel systems were developed during periods of low and high aggradation, correspondingly (Kerr and Jirik, 1990). Reservoir facies of the middle Frio, examined in core and borehole images and calibrated to well logs, showed channel filled deposits ranging from 10 to 30 ft (3 to 10 m) in thickness. (Levey et al., 1994).

The Vicksburg Formation contains siliciclastic intervals with SP and gamma-ray logs indicative of upward-coarsening grain-size profiles consistent with deltaic-dominated depositional systems. These sandstones in the upper Vicksburg Formation are commonly greater than 20 ft (6 m) in thickness (up to 80 ft or 24 m thick), and show a distinctive upward coarsening SP log profile, representative of progradational deltaic depositional environments.

The primary target for this study is the basal part of the middle Frio Formation represented by the F11 horizons (Figure 2, Chapter 1). The selection of the middle Frio Formation can give adequate gas response when modeling synthetic data from well log and seismic data. The correct AVO synthetic model with accurate gas response helps greatly to verify which noise suppression technique is AVO friendly, and how close this method can resemble the original model.

The secondary target is the Vicksburg Formation, located below the middle Frio Formation. The Vicksburg Formation contains the major fault system in the area (Hardage et al., 1996). The presence of faults is particularly important to test Structural Filter for the aspect of structure (fault and fractures) preservation.

A well-known gas producer deposited over a major faults system make the Stratton Field data the perfect choice for testing Structural Filter, which promises to preserve relative amplitude while suppressing noises, flatten seismic reflectors, and enhance stratigraphic features such as faults and fractures.

Chapter 3

Theory

This chapter presents the theory behind seismic noise suppression. The first part present the definition of noise, Signal-to-Noise Ratio (SNR), and classification of noises, while the second part describe the basic concepts of Structural Filter, Radon Filter, FK Dip Filter, and FX Decon .

3.1. Basic Concepts

3.1.1 Definition of Noise

Noise plays a crucial role in seismic data analysis. Seismic processing is strongly dependent on the quality of the records, which depends on how much noise is present. Noise in a seismic record is defined as everything that does not fit our conceptual model of the data (Russell et. al., 1990).

3.1.2 Signal-to-Noise Ratio

Signal-to-Noise Ratio (SNR) is defined as the power ratio between the signal and the background noise. It measures quality of a seismic record by comparing the level of a

clean signal to the level of background noise. Good records have high SNR, thus less obtrusive background noise. The signal-to-noise ratio is given by

$$\frac{S}{N} = \frac{P_{signal}}{P_{noise}},$$

where P is average power. Both the signal and noise power must be measured at the same or equivalent points in a system, and within the same system bandwidth. If the signal and the noise are measured across the same medium, then the SNR can be obtained by calculating the square of the amplitude ratio:

$$\frac{S}{N} = \frac{P_{signal}}{P_{noise}} = \left(\frac{A_{signal}}{A_{noise}}\right)^2,$$

where A is the root mean square (RMS) amplitude. In practice, the SNR of a seismic record is calculated by first taking the difference between the raw (observed) data minus the filtered data (signal) which give us the residual (background noise). Then, the RMS amplitude in a time window both for filtered data and residual is estimated, and SNR can be defined as:

$$SNR = \frac{S}{N} = \frac{\|df\|}{\|df-d\|},$$

where d is input signal; df is filtered signal; df-d is residual.

3.1.3 Classification of Noise

Noise in a seismic trace can be broadly divided in two categories: the coherent noise and incoherent noise. Coherent noise can be followed across several traces, while

incoherent noise (also known as random, or background noise) is unpredictable as the name implies. The coherent noises are caused by ground roll, surface reflections, and reflected refractions. Spatially repeated random noise is due to scattering from the surface, and non-repeated random noise is a result of random events, such as wind shaking a geophone or a person walking near the shot site.

The incoherent noise can to some extent be avoided in data gathering by placing geophones closely together so the difference between the two are in fact a matter of scale, (Sheriff and Geldart,1995). Differentiation of the two types can be found by looking at the frequency. The coherent noise energy is mostly low frequency due to the earth filtering, whereas random noise is mostly high frequency due to the short radiation path in the near surface (Li and Tang, 2005).

General considerations for improving seismic record quality are: looking at the coherence, the travel direction, and the repetitiousness of the noise in one trace. Noise can originate from many sources and therefore there are many types of noise. According to Dey-Sarkar and Svatek (Dey-Sarkar and Svatek 1993), there are three types of noise that distort the amplitudes in the pre-stack domain:

Type I noises are source-generated noise. These phenomena can be removed without any prior knowledge of subsurface velocities and densities. They are:

- Source generated noise
- Multiples
- Surface consistent source receiver effects

- Source signature variation with offset

Type II noise is generally associated with instrumentation or cultural noise during data acquisition. Some examples are:

- High-frequency noise
- Low-frequency noise
- Drilling noise, and
- Channel imbalance problems.

Type III noises are entirely due to wave propagation effects in a viscous-elastic medium. They are:

- Two-dimensional spherical divergence
- Thin bed attenuation
- Array attenuation
- Inelastic attenuation
- Curvature effects
- Overburden transmission effects

Each noise source has to be attenuated in a different way to get the best result. The main interests of this study are coherent linear noise, random noise, and multiples.

3.2. Noise Suppression Techniques

3.2.1 Structural Filter (SF)

Structural Filter is a dip-oriented smoothing technique used in pre-stack noise suppression that preserves edges while removing random noise. The main feature of Structural Filter is that this pre-stack noise suppression technique handles strong random noise in both flat and dipping data, removes spikes or single high amplitude events, and preserves edges (fault/fracture) and lateral Amplitude Variation with Offset (AVO).

Structural Filter works on pre-stack gathers such as Common Midpoint (CMP) gathers, Common Offset (CO) gathers, and Common Reflection Point (CRP) gathers. At the beginning of the filtering process a Running Window is chosen by the user. This window defines the number of traces for each filter pass, and its value ranges from 3 to N, where N is the maximum number of traces in a single gather. Inside the running window the algorithm scans for a local dip (Figure 6), then follows the dip orientation as a pilot, calculating the correlation factor of each trace close to the target trace (defined as the middle trace in the running window), and selects the correlation factor that best align the traces according to the true structure. The smoothing process is done by using Median Filter. After positioning traces with their true dip, median filter replaces the sample in the center of the search window by the median value of all samples within this window. With median filter, sharp discontinuities are preserved and random noise is suppressed (Figure 7). In general, the filter works in in offset (X) direction, and the running window slides down in the time axis.

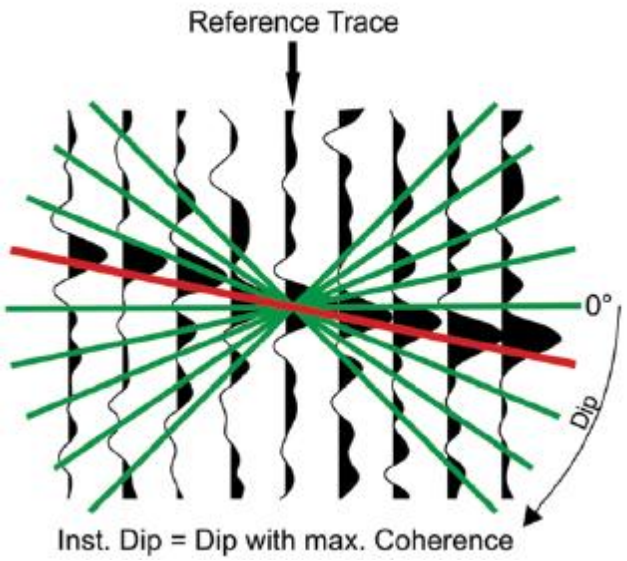

Figure 6. Schematic for the estimation of vector dip using the discrete scan method. In this method the coherence is calculated along a discrete number of dips. The number of adjacent traces, as well as the vertical range used in the estimation can be varied. (Modified from Eichkitz et al., 2012).

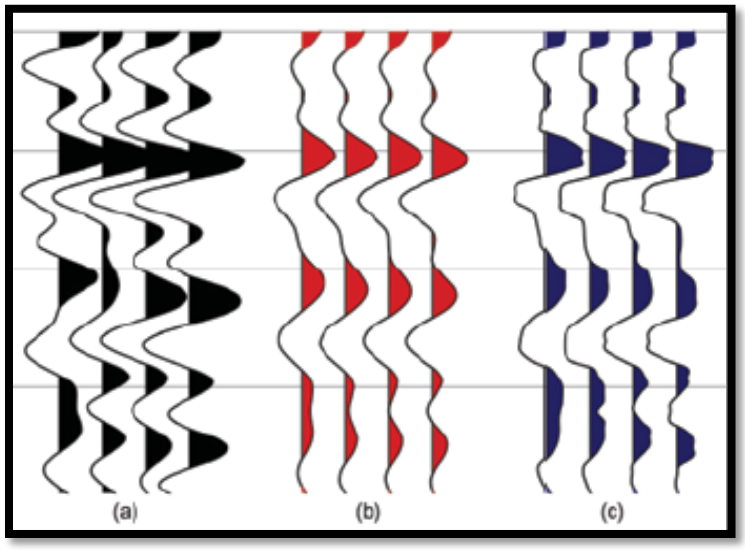

Figure 7. Schematic showing the effect of filters applied on seismic amplitude traces (a). All filters are calculated using a 3x3 search window. The simplest filter is the low-pass (mean) filter (b). It simply averages the data and by that suppresses random noise, but it also smears short wavelength events. The median filter (c) replaces each sample by the median of the samples within the analysis window. By doing this, it suppresses noise but preserves sharp discontinuities. (Modified from Eichkitz et al., 2012).

3.2.2 Radon Transform (Radon Filter)

In the Radon transform technique the data are modeled as a series of curved trajectories. Primary reflections and multiples can be separated in Radom domain if there is a specific range of move-out for multiples. Once this specific range of move-out is identified in the tau-p domain they are removed, and theoretically there are no multiple events in the signal.

The forward transform is a series of linearly skewed sums. In general, we may write the following straightforward equation to indicate the meaning of p:

$$t = T + pX,$$

where, X = offset, T = time at zero offset, t = time at offset X, and p= moveout term.

This equation tells us that a linear event with a dip of p millisecond per trace and zero-offset intercept Tau will transform to a point at time t and movement p after a tau-p transform (Figure 8). In the inverse tau-p transform, points transform to straight lines with the indicated moveout.

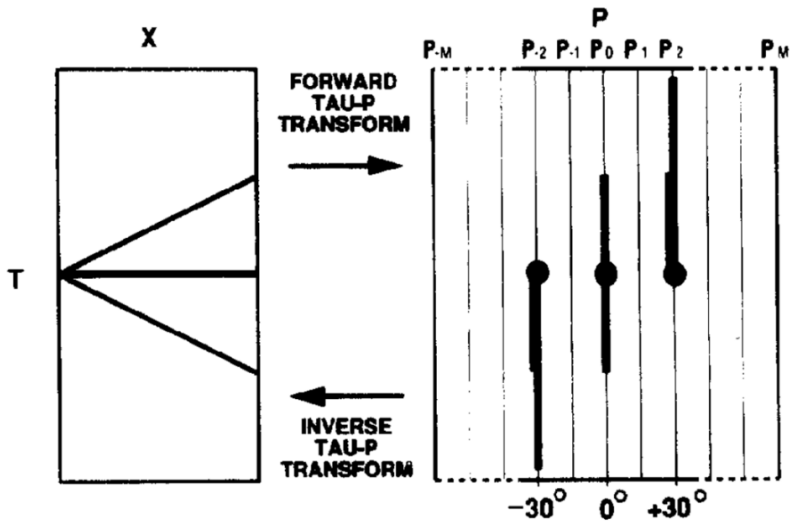

Figure 8. Schematic showing that a linear event in T-X domain will be a point after Tau-p transform. (Modified after Russell et al., 1990).

Besides the linear curve there are two common nonlinear curves that are of interest to us in seismic processing: the parabola and the hyperbola. The respective equations are:

$$t = \tau + pX^2$$

and

$$t = (\tau^2 + p^2X^2)^{1/2},$$

The notation is the same as in the equation used earlier in the tau-p transform with one exception: in the equation for the parabola, p is slowness divided by distance in s/m^2 or s/ft^2, while in the linear and the hyperbola equation can be thought of as slowness or inverse velocity in s/m or s/ft.

Each of the curves represented by the three equations has its own advantages and disadvantages. For example, the straight line can be used for modeling any events with linear moveout. However, it falls down when we try to model hyperbolic NMO curves.

For the hyperbola case, the introduction of the square root operation makes this a highly nonlinear equation and therefore difficult to formulate on a computer. The ideal compromise is the parabolic curve which displays curvature but does not involve taking a square root.

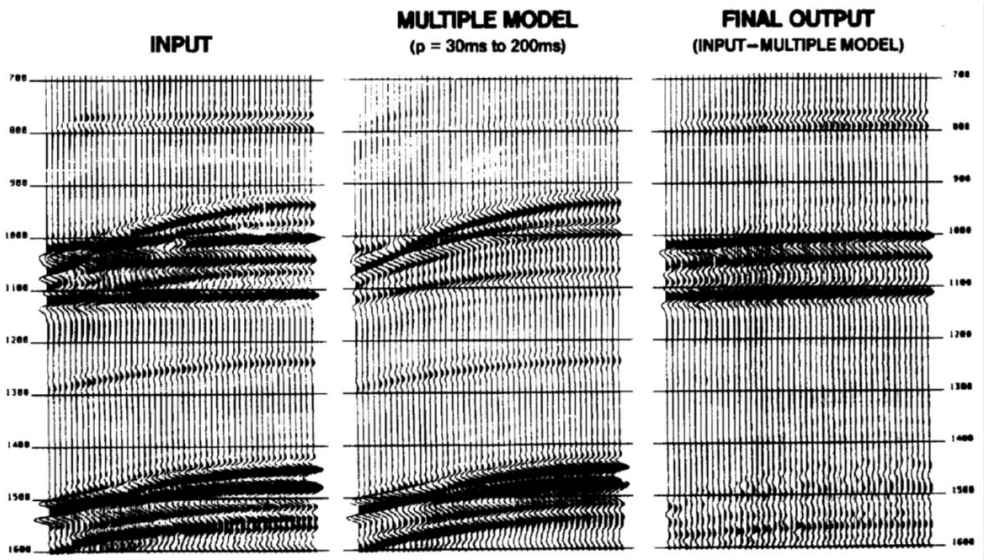

Figure 9. Multiple suppression using Parabolic Radon Transform (Modified after Russell et al., 1990).

Figure 9 shows an example using parabolic radon transform to remove multiples from seismic data (modified from Russell et al., 1990). This method can work very well to suppress multiple energy and conserve the primary, with the only exception being that it reduces the reflection amplitudes at near and far offsets due to a truncation effect (Nowak and Imhof, 2006), which is not desired for AVO analysis.

3.2.3 Frequency-Wavenumber (FK) Dip Filtering

Coherent linear events in the t - x domain can be separated in the f - k domain by their dips. This allows us to eliminate certain types of unwanted energy from the data (Figure 10). In particular, coherent linear noise in the form of ground roll, guided waves, and side-scattered energy commonly obscure primary reflections in recorded data. These types of noise usually are isolated from the reflection energy in the f - k domain.

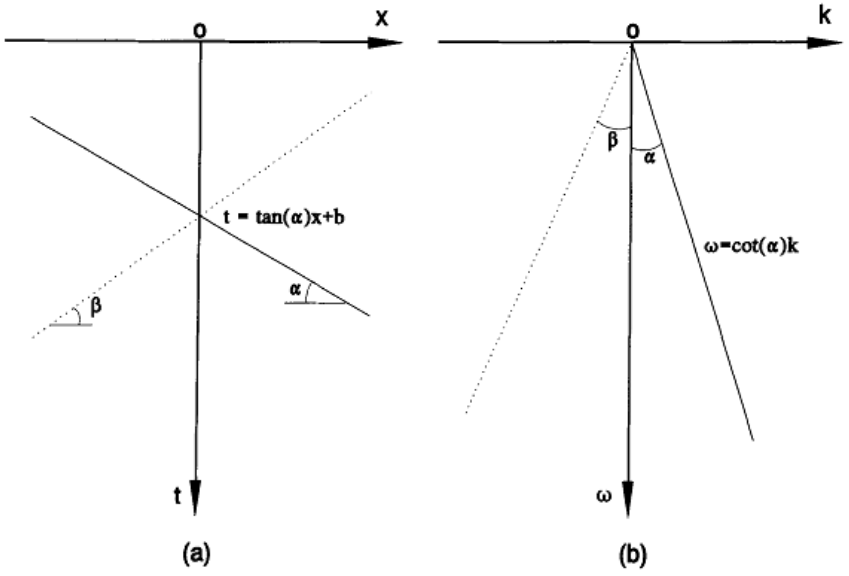

Figure 10. Schematic illustration of dip separation in the f-k domain (b) for dipping events in the x-t domain (a). Modified from Ogiesoba et al., 2011.

A typical application of FK Dip Filter is ground-roll attenuation. Ground roll is a common linear coherent noise. It consists of dispersive waveform that propagates along the surface and is low-frequency, large-amplitude in character. Typically, ground roll in the F-K spectrum of a shot gather are the low-frequency and large-amplitude events close to the wavenumber axis, and reflections are situated around the frequency axis. Based on this characteristic, a fan-like window is imposed on this spectrum within which the

undesired energy is rejected. This is followed by inverse mapping back to the t - x domain. The resulting filtered record is largely free of ground-roll energy.

Defining a reject fan in the f - k domain is one implementation of the process known as f- k dip filtering. Note that dip filtering is but one type of f – k filtering. The reject zone in the f - k domain may be specified as not just like a fan but also as a shape suitable for the objective in mind. For instance, the reject zone may be defined as one entire quadrant of the f - k plane in the case of multiples attenuation. It may only be one half of one quadrant in the case of a spatial antialiasing filter.

In this study, the steps involved in f - k filtering are the following:

(a) Starting with a common-offset gather, apply 2-D Fourier transform.

(b) Define a 2-D reject zone (Arbitrary polygon) in the f - k domain by setting the 2-D amplitude spectrum of the f – k filter to zero within that zone and set its phase spectrum to zero.

(c) Apply the 2-D f- k filter by multiplying its amplitude spectrum with that of the input data set.

(d) Apply 2-D inverse Fourier transform of the filtered data.

3.2.4 FX Deconvolution (FX Decon)

This method is used when random noise is present or when coherent noise can be viewed in a random domain, and was introduced by Canales (Canales, 1984). The FX Decon prediction process depends on the form of linear events in frequency versus space direction (Figure 11). Given linear seismic event in time domain,

$$f(x) = \delta(a + bx - t)$$

In predicted deconvolution they are transferred to the frequency-space (F-X) domain by taking the forward Fourier Transform of each trace.

$$f(\omega) = e^{i\omega(a+bx)}$$

or

$$f(\omega) = e^{i\omega a}\cos(\omega bx) + i\sin(\omega bx)$$

To predict linear events the least square prediction filter can be calculated by the matrix equation

$$d = Xf$$

where:

$d = [x_2, x_3 \ldots\ldots x_{n+1}]$ is the desired output build by shifting one sample of the input data,

f is Predicted Error Filter (PEF) and can be expressed as $f = (X^*X)^{-1}X^*d$,

X is the complex autocorrelation function, and

*X** is the complex conjugate transpose of *X*.

The F-X prediction is applied to small windows to ensure that events are locally linear, and that the data within each window are then Fourier transformed. For the spatial series created at each frequency by the Fourier transform, a prediction filter is calculated. Each calculated filter is first applied forward and then reversed in space, with the results averaged to maintain a symmetrical application, as in the T-X prediction case. (Abma and Claerbout, 1995; Gulunay et al., 2001).

The FX Deconvolution prediction can also be found by taking the Wiener Filter for each frequency (Canales, 1984; Hornbostel, 1991). The design of a Wiener Filter requires that the difference between the filtered signal and some desired output signal have a minimum mean-squared error (Bikel and Martinez, 1983). In practice pre-stack F-XY decon is the third dimension extension of FX Decon.

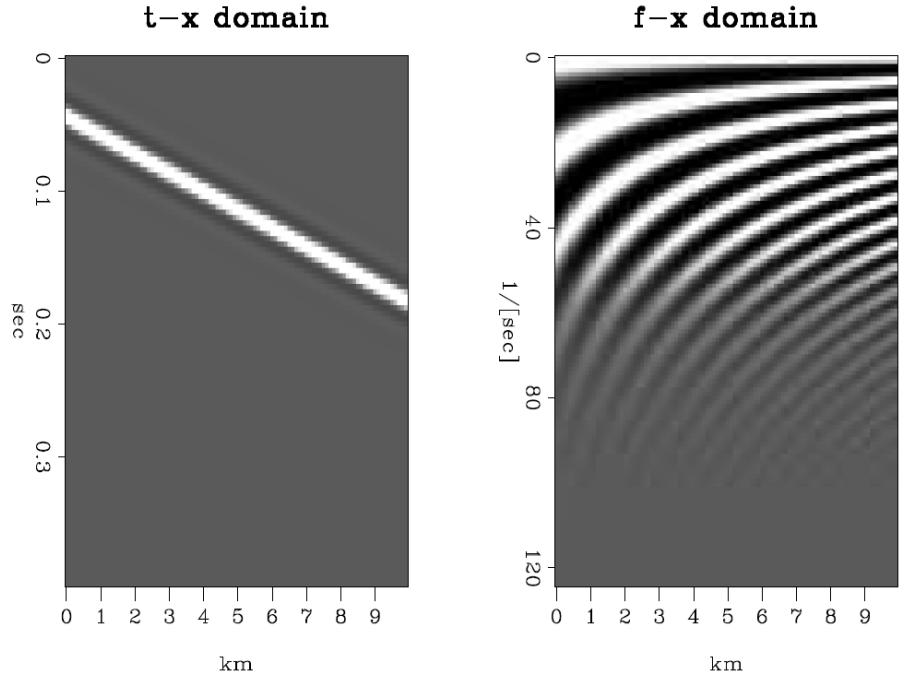

Figure 11. Single dip in Time and Fourier transformation domain. In the Fourier domain the signal is periodic along any horizontal line. Thus, primaries are simple to model, and random noise can be removed easily (Modified After Abma and Claerbout 1997).

Chapter 4

Methodology

This chapter presents the methodology used for this thesis. First is a description of the data used in this study, followed by the general workflow which includes synthetic study and real data application. Finally, the software used during this investigation is presented.

4.1. Data set

To test the different noise suppression techniques in this study, they will be evaluated and compared in both synthetic and real data. The real data used to test Structural Filter is 3D seismic and well log data set from Stratton Field in Nueces County, Texas. It covers an area of approximately 2 mi^2 (5.2 km^2) and contains a large number of wells that were drilled and used for making a geologic analysis of the Frio Formation, a major reservoir. Most of the Frio reservoirs are less than 15 ft (5 m) thick and they are vertically separated by only 10-15 ft (3-5 m). The seismic interpretation at Stratton Field was particularly challenging because of the thin and closely stacked reservoirs.

The pre-stack data used to evaluate Structural Filter are NMO corrected CRP gathers. The processing sequence used meets the basic requirements of true amplitude processing or preserved amplitude processing. Basic theories and algorithms describing such AVO

compliant processing procedures are abundant in the literature. The major steps in the true amplitude processing to generate CRP gathers are:

- Input Data (SEG-Y)
- Geometry application and QC
- Air Blast Attenuation (ABA)
- True Amplitude Recovery (TAR)
- Surface Consistent Amplitude Compensation (SCAC) for sources, receivers and offset
- Surface Consistent Deconvolution
- Refraction Statics Corrections
- Velocity Analysis
- Surface Consistent Residual Statics Corrections
- Normal Moveout (NMO) Correction
- F-XY Decon Pre-stack
- 3D Kirchhoff Pre-stack Time Migration
- CRP gathers generation

4.2. General Workflow

The present study mainly consists of two stages, synthetic study and real data application. Synthetic data helps to quantitatively assess and compare the different noise suppression techniques and prove the advantages of Structural Filter over other methods; application in seismic data would show how Structural Filter has been applied to real data, what kind of improvement can be achieved in the filtered volume and how the conditioned data helps in AVO analysis. The general workflow is presented in the following chart:

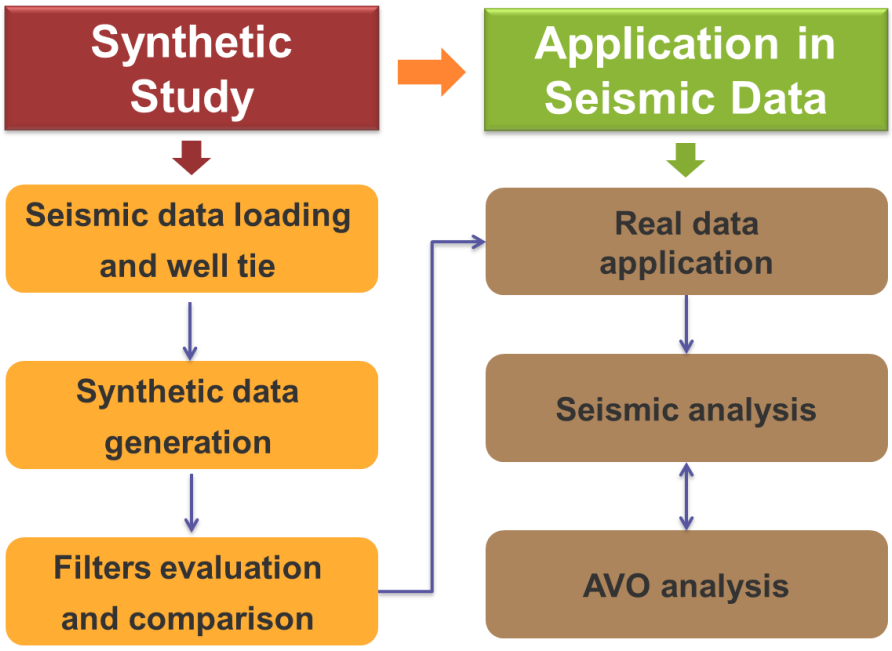

Figure 12. General Workflow applied in this study.

The general workflow presented in Figure 12 shows the two main steps in this study: Synthetic Study and Real Data Application. A detailed description of each step will be explained in the next two sections.

4.2.1 Synthetic Study

The advantage in testing noise suppression methods with synthetic data is that we know exactly the signal and the noise, which helps in analyzing the methods quantitatively.

The synthetic data was generated from a single well AVO modeling using Hampson-Russell® software package. Since there is no availability of sonic logs, a pseudo-sonic log was computed from resistivity data using Faust's relation (Faust et al., 1951). In addition to Faust approximation, local correction in gas-bearing zone was applied using time average equation (Wyllie et al., 1956), and Raymer-Hunt-Gardner (RHG) equation. Comparing the two pseudo P-wave curves, it was decided to use RHG to correct the gas sand velocity. The reasons are:

1. At 6330 ft (1929 m) depth, the formation is relatively unconsolidated sandstone. Wyllie will overestimate the sonic velocity in an unconsolidated formation, the alternative is RHG equation.
2. In general, porosity values within the gas zone are lower than 37%, which is consistent with RHG equation's assumption.

After a pseudo sonic log was created, well tie was performed with seismic data (Figure. 13). The well calibration correlation coefficient is 0.808 for well- 9, which indicate an excellent well – seismic tie. After the well calibration, P-wave, S-wave, and Poisson Ratio log was calibrated and calculated. S-wave was calculated using mud rock line (Castagna et al. 1985), which assumes that the calculated S-wave velocity is correct for brine-filled rock. Because the in-situ fluid is gas, correction was done on the S-wave

velocity to make it representative of a gas-saturated case. At the target zone (around 1580 ms), fluid substitution was carried out by applying Gassmann's equation. The input fluid parameters for gas-saturated case were V_p= 88.71 us/ft; Φ= 0.27; ρ= 2.44 g/cc; V_s = 132.30 us/ft; S_w= 30%; σ = 0.09. These parameters are the result of direct calculation from well logs.

AVO modeling was done by using Elastic Wave algorithm. The Elastic Wave modeling algorithm, unlike Zoeppritz and Aki-Richard model, takes into account inter-bed multiples and converted waves besides the primary reflections in a complex layered medium. Because converted waves and multiples through reflecting layers may affect the AVO response at the target and create P-wave reflections displaying a completely different AVO response than those from a single elastic interface, one should model the pre-stack seismic amplitude and the waveforms using the full elastic wave modeling algorithm (Simmons and Backus, 1994).

Figure 14 shows the synthetic CMP gather after AVO modeling. The result indicates an AVO class III response, which by definition is an AVO anomaly associated with amplitude increase with offset (Rutherford and Williams, 1989).

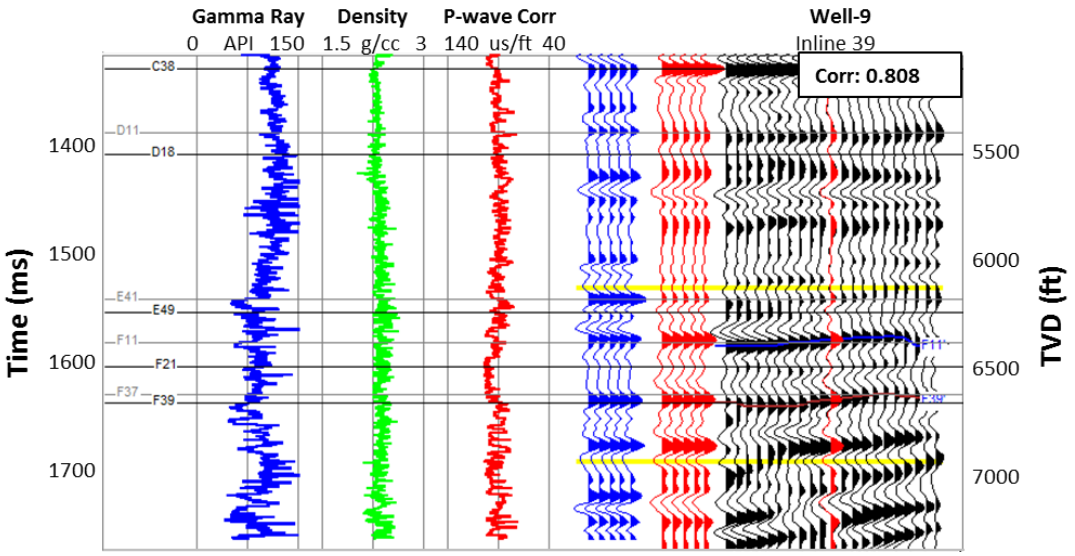

Figure 13. Well calibration with seismic data for well- 9. The correlation coefficient is 0.808.

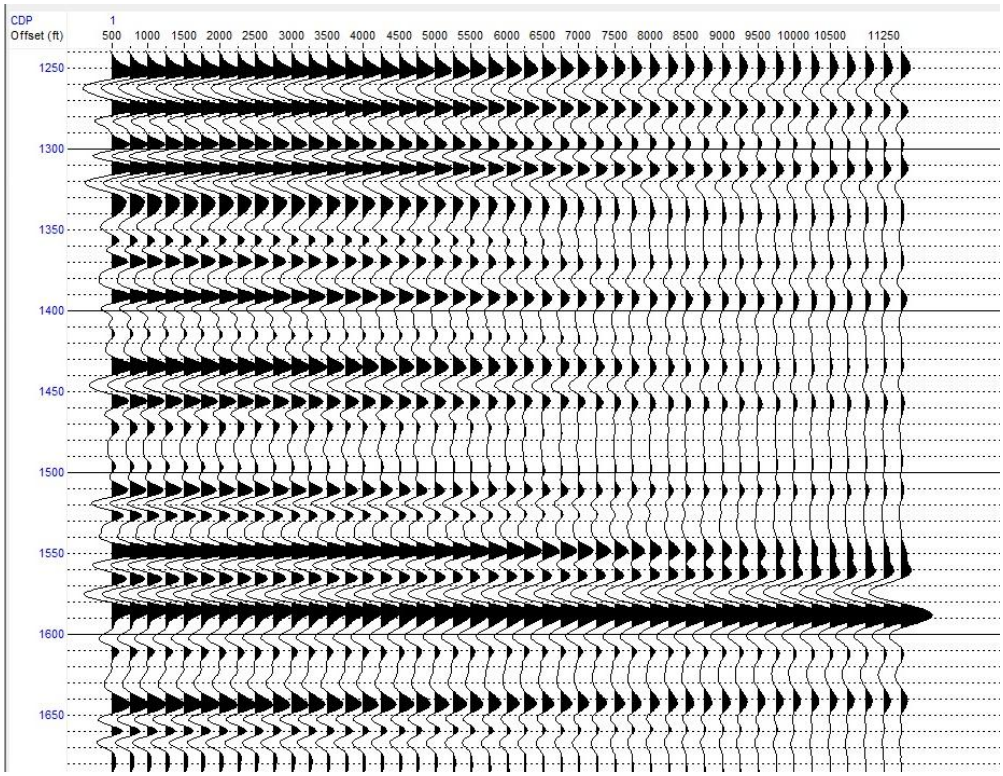

Figure 14. Synthetic gather generated using single well modeling. Notice that the selected parameters gave an AVO class III response at about 1580 ms, the target zone .

In order to test the two version of Structural Filter, pre-stack and post-stack, the generated synthetic data was separated in both Common Midpoint (CMP) and Common Offset (CO) domain. In Common Midpoint domain three kinds of noise were added: multiples, spikes, and random noise. Multiples were modeled as uncorrected primary events. Spike noise was added in the middle of the CMP gather with peak amplitude three times that of the input trace. Random noise amplitude was set to be 66% of the signal. In Common Offset domain, linear dip noise and random noise were added. For linear noise, the added dipping angle was 45 and 60 degrees. Random noise amplitude was set to be 66% of the signal. In addition to the noise, a dipping fault was added with a time shift of 20 ms approximately.

After synthetic data were generated for the Common Midpoint and Common Offset domains, it was time to test the different noise suppression techniques. The workflow applied for this step is shown in Figure 15.

The workflow showed in Figure 15 is designed for the synthetic study. The evaluation process begins with input data. The input volume is 81 CMP gathers (9 inline by 9 crossline) built by repeating the synthetic gather (created from the previous step) in both Common Midpoint and Common Offset domains.

In CMP domain, the input synthetic gathers described previously are Normal Moveout (NMO) Corrected. Pre-stack Structural Filter is applied to the input synthetic gathers alone and to the input synthetic gathers with padded intercept in front of the data (a detailed explanation about how to extract and pad intercept can be found in Appendix B). Radon Filter is applied to the input synthetic gathers with a combination of primary

pass and multiples suppression.

In CO domain, the input common offset gathers were processed by post-stack Structural Filter, FK Dip Filter, and FX Decon, and three sets of filtered gathers were evaluated.

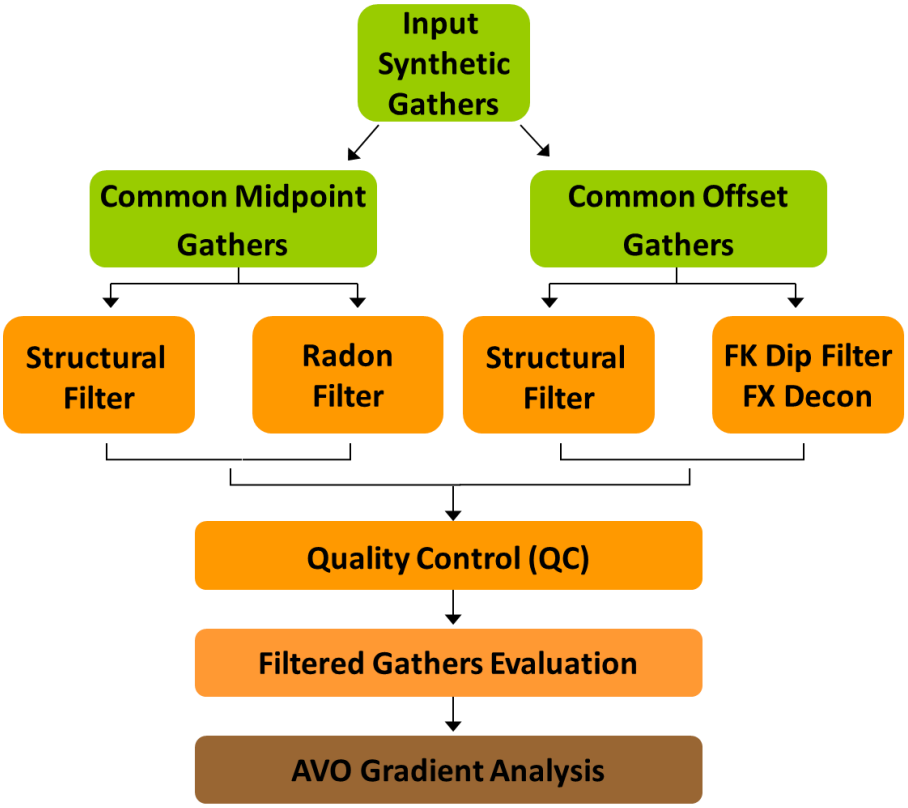

Figure 15. Workflow applied for the Synthetic Study.

Quality Control (QC) mainly consists of residual calculation, Signal-to-Noise Ratio (SNR) estimate, and AVO curves plot and overlay. The residual calculation refers to the difference between input data and filtered data, a standard method in any case where a de-noising filter is applied to an input data. The residual allows us to quickly estimate the efficiency of the filter, by answering questions such as: what kind of noise has been suppressed, in what percentage, and if there is any damage to the signal.

The estimated Signal-to-Noise Ratio (SNR) is one of the key parameters which allowed us to quantitatively assess the noise suppression techniques. In general, an increase in Signal-to-Noise Ratio (SNR) should be observed after a filter is applied.

In order to determine which noise suppression technique is an AVO compliant method, AVO curves are plotted for each gather before and after each filter application. The AVO gradient analysis is carried out to determinate how well each curve fits the theoretical two-term equation described by Aki and Richards (Aki and Richards, 1985). After individual evaluation, their AVO curves are overlaid. These kinds of plots allow us to answer questions such as how well each filter works in term of amplitude preservation and which filter is the best choice for AVO data conditioning.

The evaluation and comparison process assesses each method based on its performance within all the parameters previously described. The best method should deliver data with high signal and noise ratio, preserve amplitude with offset variation, and be free of random and/or linear coherent noise. If the data does not satisfy one of the above mentioned criteria, an update of filter parameters should be done to re-generate new sets of filtered gathers. This process must be iterated as many times as necessary until a satisfactory result is obtained.

4.2.2 Real Data Application

The application of Structural Filter in seismic data depends on the real situation of each dataset. For Stratton Field data, an adapted workflow was designed based on the evaluation of data quality including: signal-to-noise ratio, type of noise, presence of fault, and dipping events. The workflow applied is showed in Figure 16.

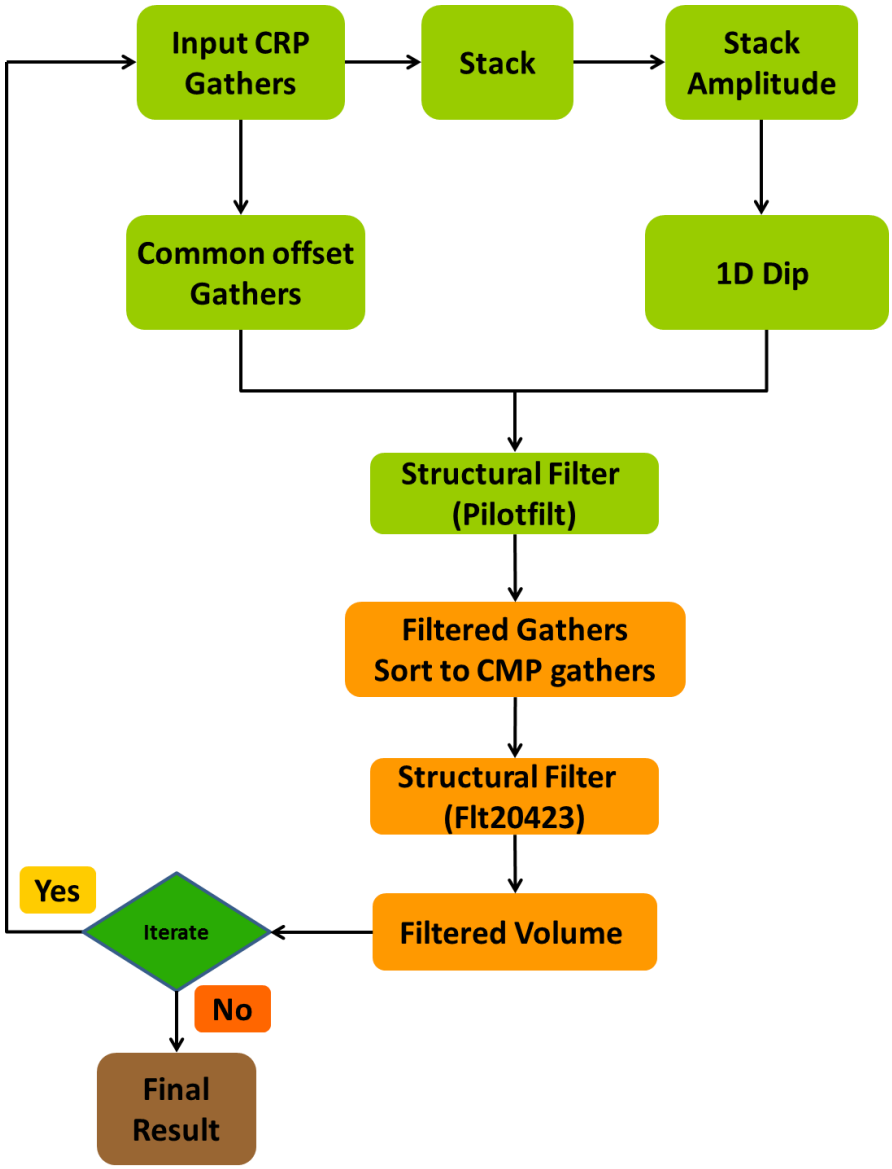

Figure 16. Workflow for Real Data Application. Modified from AASPI, Murfurt K. 2011.

The workflow shown in Figure 16 is designed for the application of Structural Filter to seismic data. The first pass of Structural Filter was done in Common Offset domain, whereas the post-stack version of Structural Filter (Pilotfilt) was applied to input CRP gather sorted into common offset gathers. The same input CRP gather is stacked with the best velocity and statics to meet the need of the filter that requires a pilot stack, and to obtain the dip information from the amplitude data.

The second pass of Structural Filter was done in CMP domain. The pre-stack version Structural Filter (flt20423) was applied to output from the last step and sorted into CMP gathers with padded intercept at front.

All filtered volumes were judged by the same quality control criteria to determine whether they became the final result, or if they need to iterate with an updated parameter.

Chapter 5

Results and Discussion

This chapter presents the results obtained in this study. First, the results of how Structural Filter performed in synthetic evaluation; second, the application of Structural Filter in Stratton Field data and comparison of the results with Radon Filter, FK Dip Filter, and FX Decon.

5.1 Synthetic Study

The Synthetic Study consists of two main comparisons: first, in Common Midpoint domain, and second, in Common Offset domain. The results showed are focused on how Structural Filter performed by analyzing synthetic gathers with Amplitude plots, AVO curves, and AVO gradient analysis. Comparisons of Structural Filter with other methods are presented for gathers and AVO curves.

5.1.1 Common Midpoint Domain

In common midpoint domain pre-stack Structural Filter was applied to CMP gathers. Figure 17 (a) showed the input clean model exhibiting Class III AVO response at the target, around 1580 ms. In this domain, three types of noise were added to the clean model as explained previously in Chapter 4, Synthetic Data Study: multiples, spikes, and

random noise (Figure 17 b). The calculated Signal-to-Noise Ratio (SNR) for noisy gather is 0.7989. Figure 18 showed the input noisy gathers, output gather after Structural Filter and their residual. For a better understanding of this result, an amplitude plot was done at the target horizon (around 1580 ms), to see how AVO response changed after filter application.

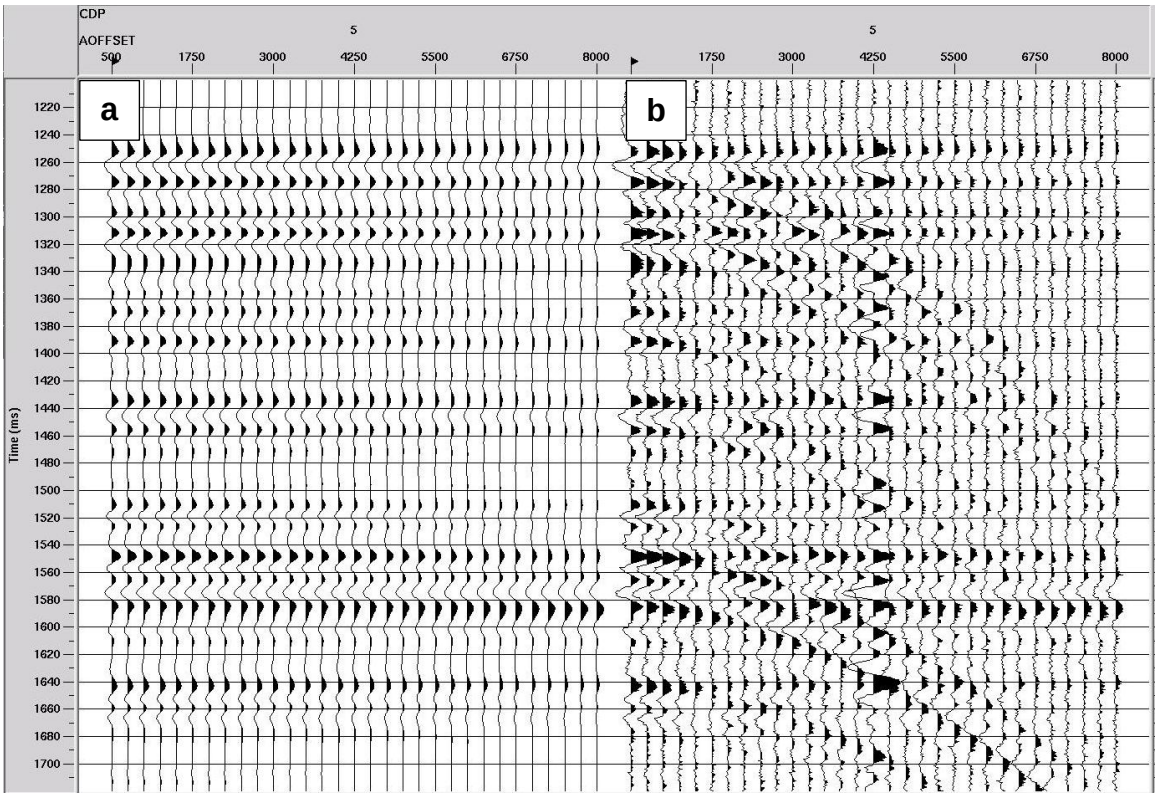

Figure 17. a) Synthetic gather generated using elastic wave AVO modeling. b) Synthetic noisy gather. SNR = 0.7989.

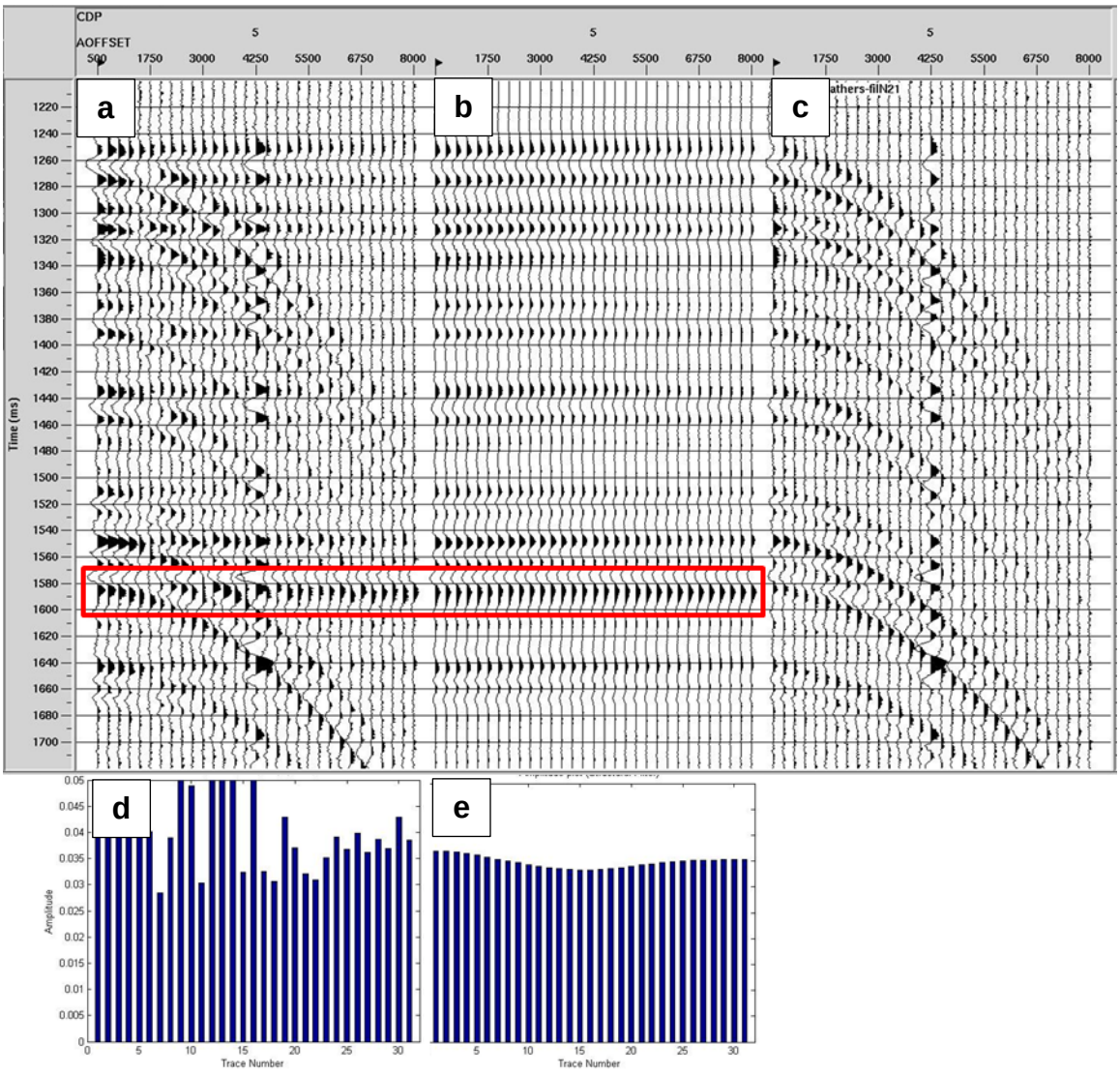

Figure 18. a) Input noisy gather, b) Structural Filter, c) Residual, d) Amplitude plot for noisy gather and e) Amplitude plot for SF filtered gather. The amplitude plot was extracted from the target horizon (red rectangle). Signal-to-noise ratio for filtered gather after Structural Filter is SNR = 3.3025.

Structural Filter suppressed random noise, spikes, and multiples with high efficiency. It trimmed the reflection amplitude but did not preserve AVO signature, especially at near offset when compare to the input clean model. For parameters used in Structural Filter and all other methods please refer to Appendix A.

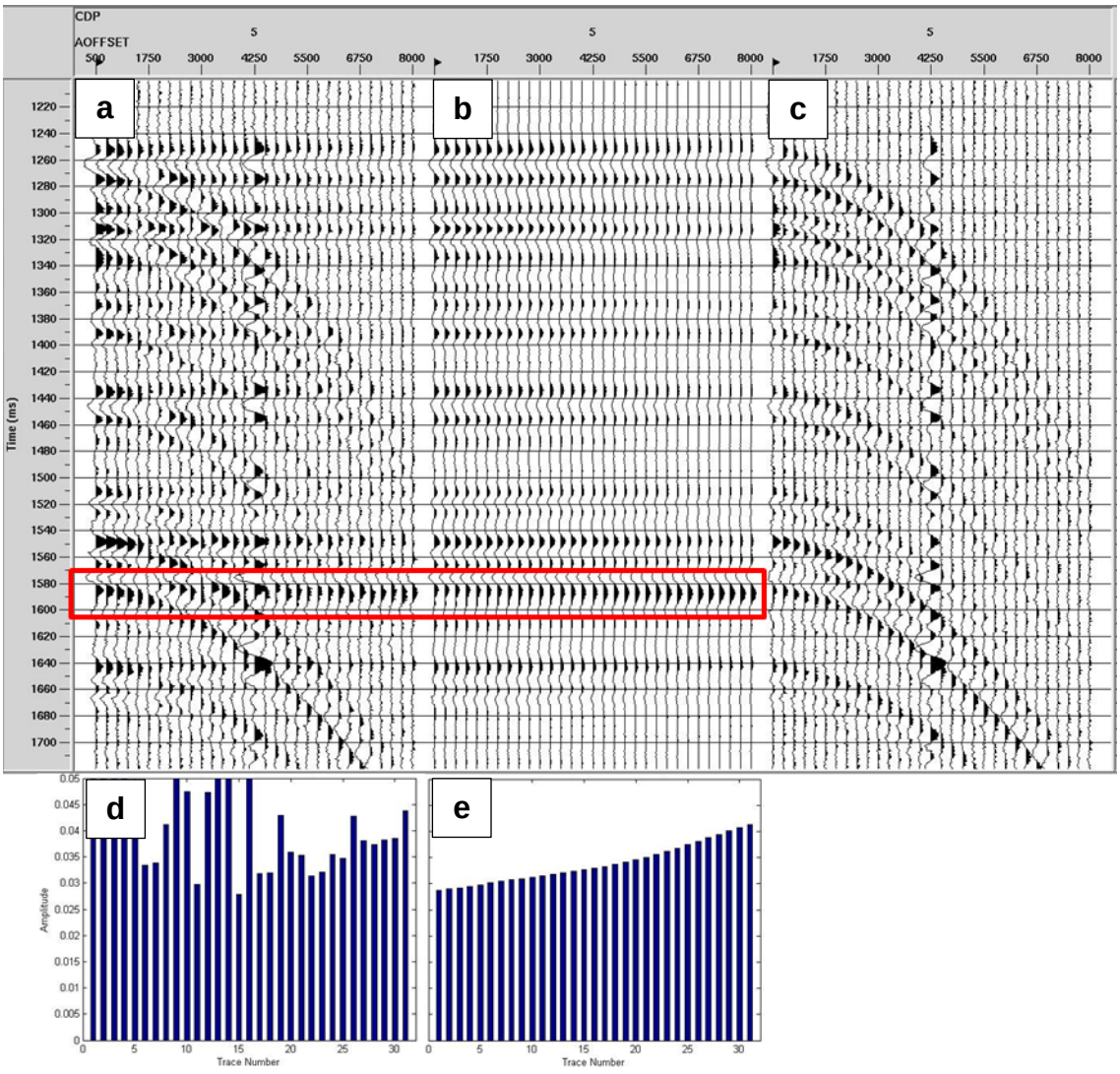

Figure 19. a) Input noisy gather, b) Structural Filter, c) Residual, d) Amplitude plot for noisy gather and e) Amplitude plot for SF filtered gather. the amplitude plot extracted from the target horizon (red rectangle). Signal-to-noise ratio for filtered gather after Structural Filter with padded intercept is SNR = 4.2808.

Figure 19 shows that Structural Filter applied to noisy gather with padded intercept suppressed random noise, spikes, and multiples with high efficiency. It fixed the near offset amplitude overestimate problem, preserved the reflection amplitude, and revealed AVO signature that exists in the input clean model. A detailed explanation about how to extract and pad AVO intercept can be found in Appendix B.

5.1.2 Common Offset Domain

In common offset domain, post-stack Structural Filter was applied to common offset gathers with pilot-stack. Figure 20 a) shows the input clean model and Figure 20 b) shows the input noisy model which added linear noise, random noise and a dipping fault to the clean model as described previously in Chapter 4, Synthetic Data Study. The calculated SNR for noisy gather is 0.9587.

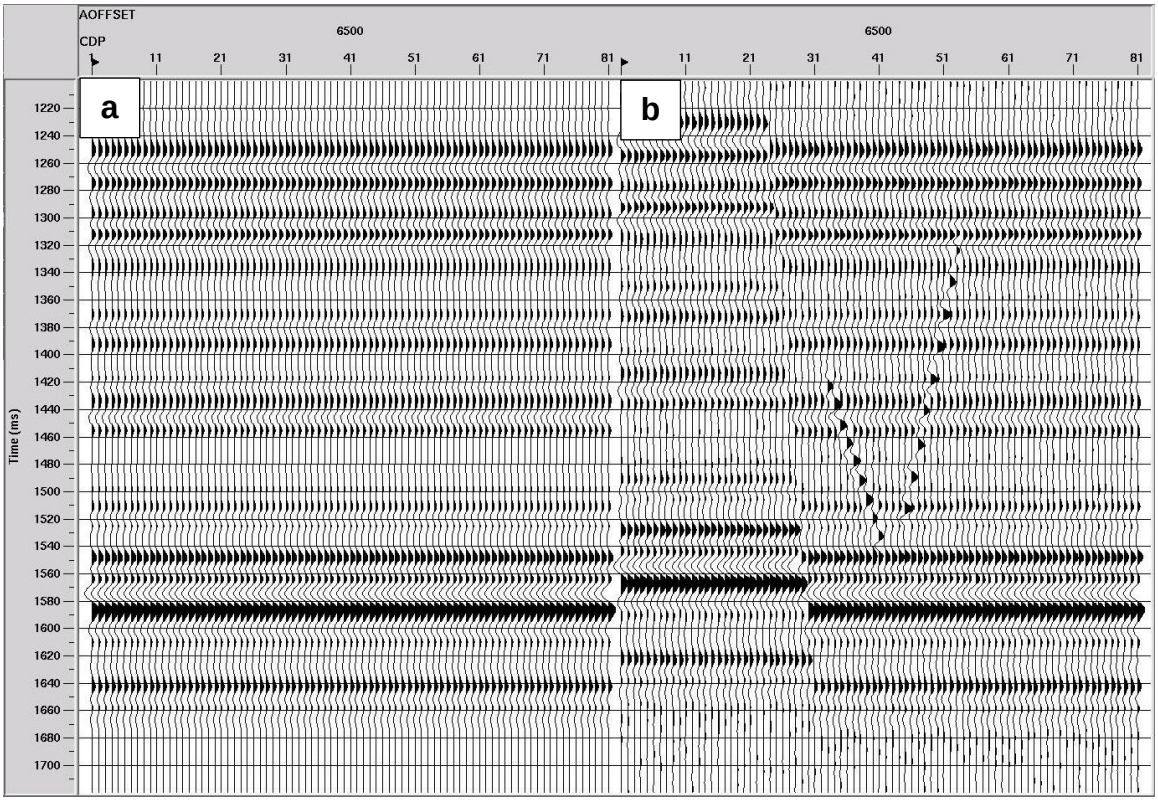

Figure 20. a) Input clean model; b) Noisy gather. SNR = 0.9587.

Figure 21 shows the offset section on offset 6500 before and after Structural Filter. Across faults, the filter presented smearing effect; this effect can be adjusted to the minimum. However, by improving the fault smearing, random noise reduction will be lowered. That suggests a tradeoff between fault detection and noise reduction. The

parameter that controls this aspect of the filter is Fault Detection Threshold (Thr). Figure 22 and 23 present the filter results for different values of Fault Detection Threshold. Observe how the results vary as this parameter is changed.

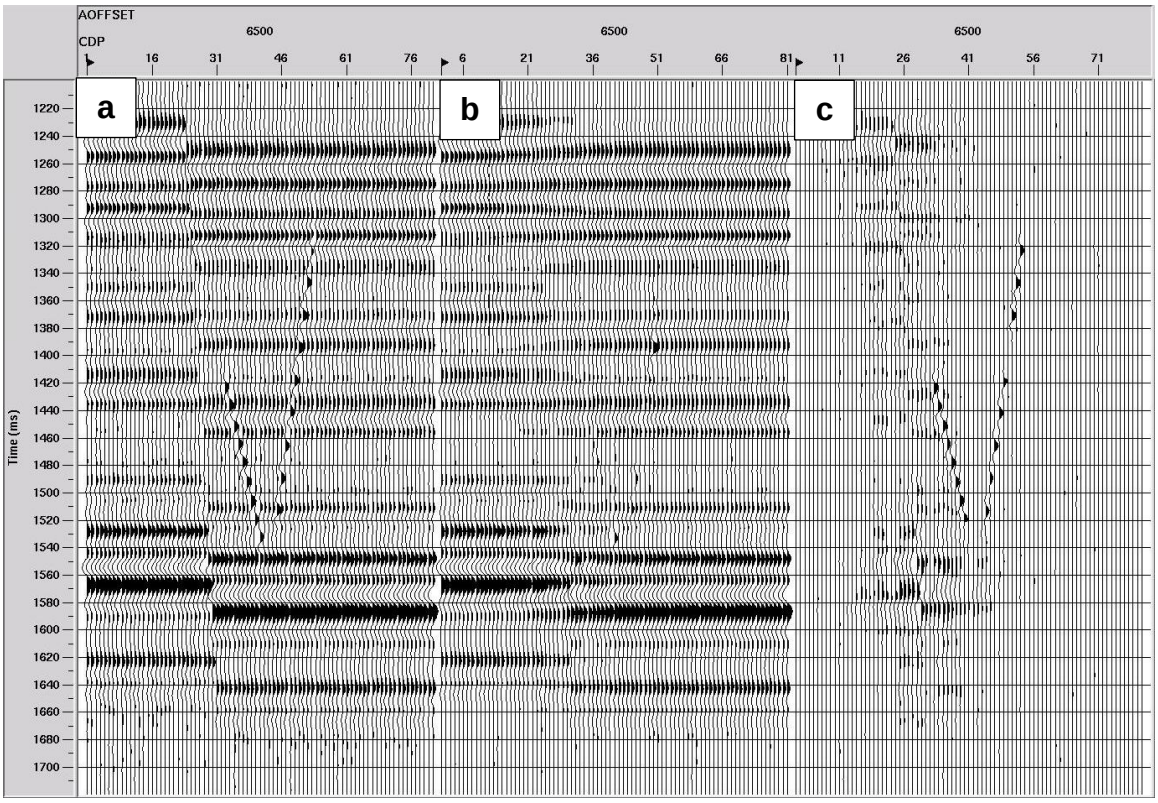

Figure 21. Offset section on offset 6500. a) Input noisy model, b) Structural Filter and c) Residual. Thr =1.0. SNR = 1.3125.

Observe the offset section in Figure 21, linear noise was fairly suppressed but not completely. The smearing effect across fault is small using this parameter, it decreases if the Fault Detection Threshold is reduced (Figure 22). However, with a small Fault Detection Threshold noise suppression power is limited (Figure 23).

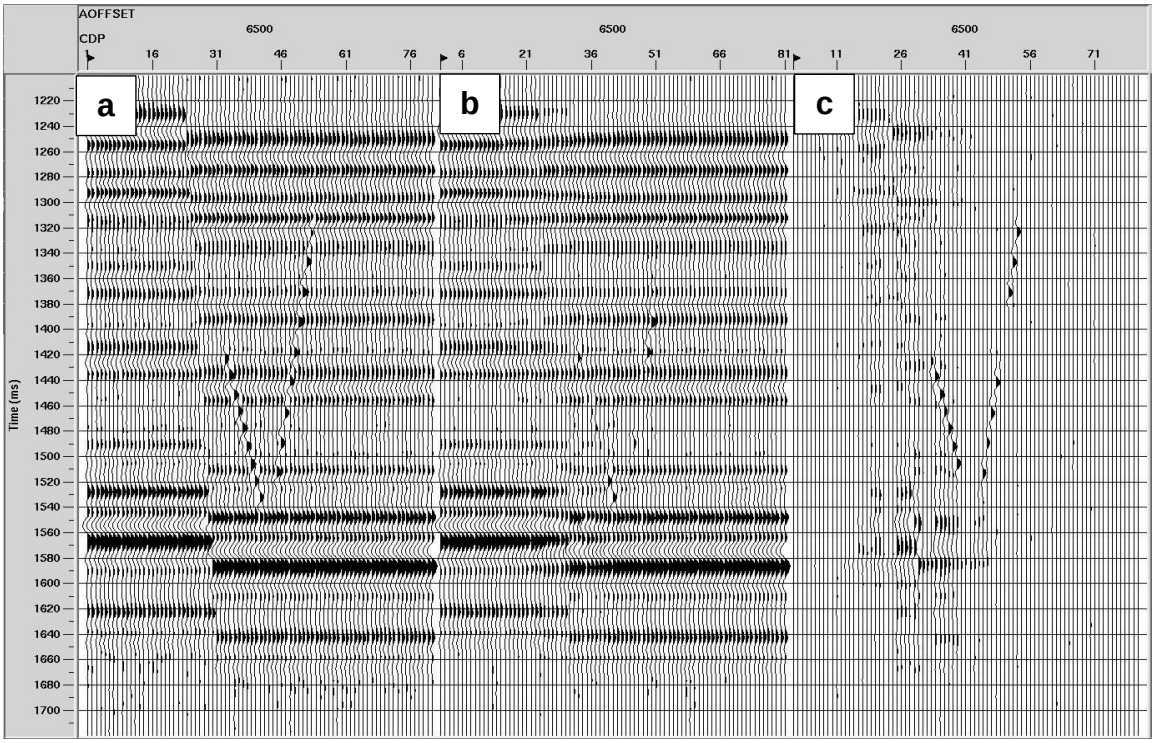

Figure 22. Offset section on offset 6500. a) Input noisy model, b) Structural Filter and c) Residual. Thr =0.5; SNR = 1.2789.

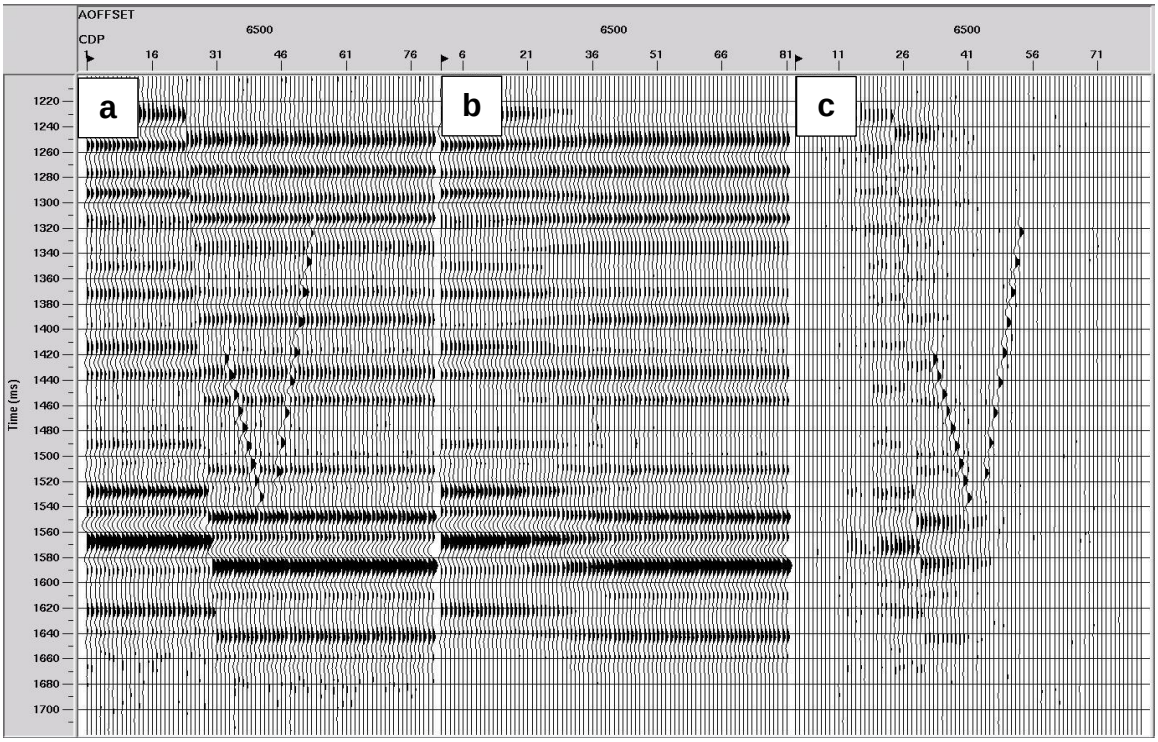

Figure 23. Offset section on offset 6500. a) Input noisy model, b) Structural Filter and c) Residual. Thr =4.0; SNR = 1.3789.

After comparing the different outcomes of Structural Filter by changing the Fault Detection Threshold, it was decided that using Thr = 1 produced the best relation between fault detection and noise suppression.

In order to compare with the results from previous subsection, common offset filtered gathers are resorted into CMP gathers. The following figure shows pre-stack Structural Filter, the best result from CMP and CO domain, compared with Radon Filter, FK Dip Filter, and FX Decon.

In Figure 24, all filters suppressed random noise with high efficiency. Radon Filter did not preserve reflection amplitude at near and far offset; FK Dip Filter applied to noisy gather fairly preserved the reflection amplitude, with the exception that it boosted the amplitude at near offset; FX Decon did not preserve reflection amplitude; Structural Filter applied to noisy gather preserved reflection amplitude, revealed AVO signature (amplitude increases with offset) that exists in the input clean model, and it produced the highest Signal-to-Noise Ratio, SNR=4.28.

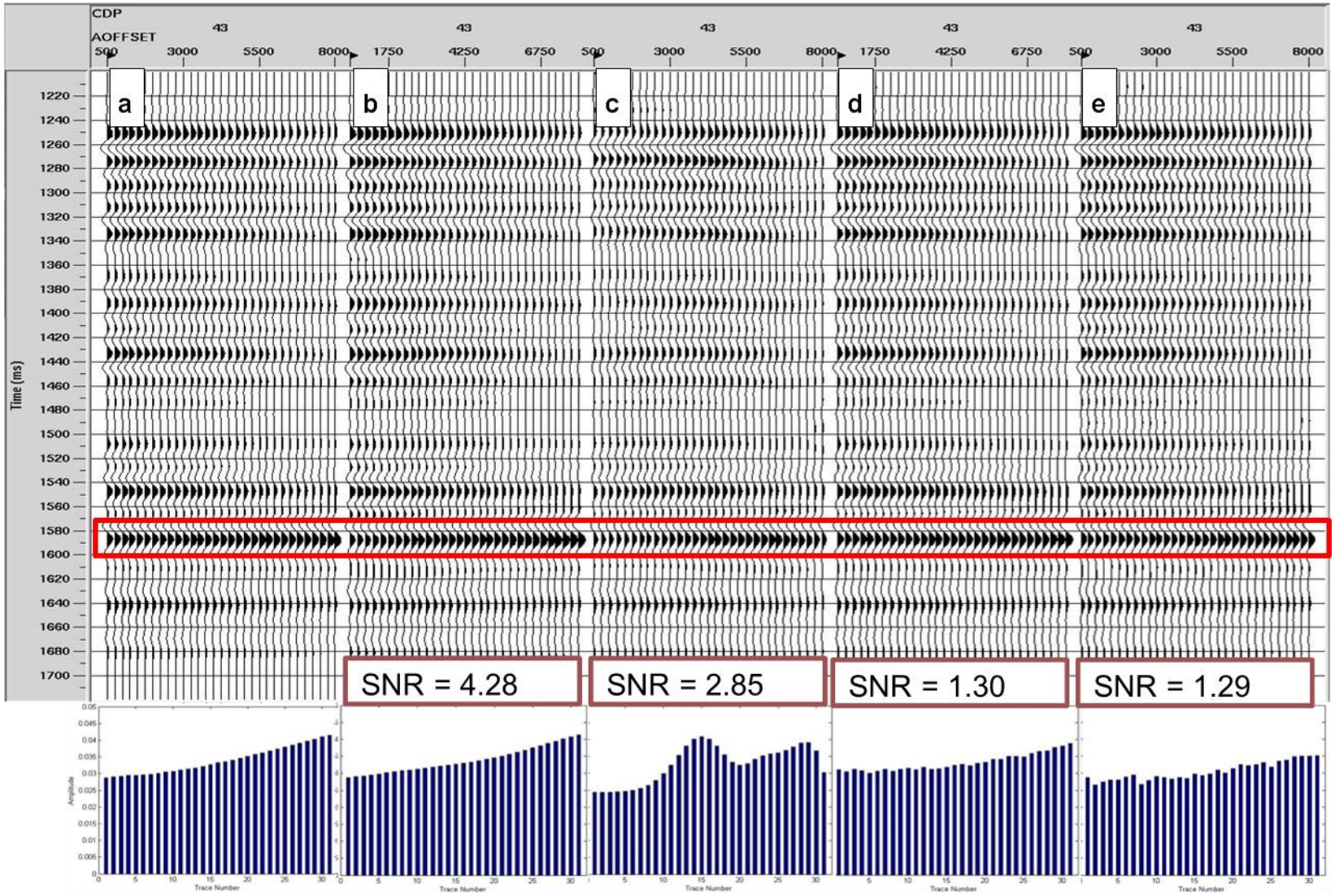

Figure 24: Input clean model a) Structural Filter b) Radon Filter c) FK Dip Filter d) and FX Decon e).

To better illustrate the effects of each noise suppression methods on trace amplitude, AVO curves at the target zone was plotted. In Figure 25 the plotted curves are clean model, Structural Filter, Radon Filter, FK Dip Filter, and FX Decon. These curves are calculated using RMS amplitudes normalized with the average value of each array. Amplitude values are from 1580 ms to 1599 ms.

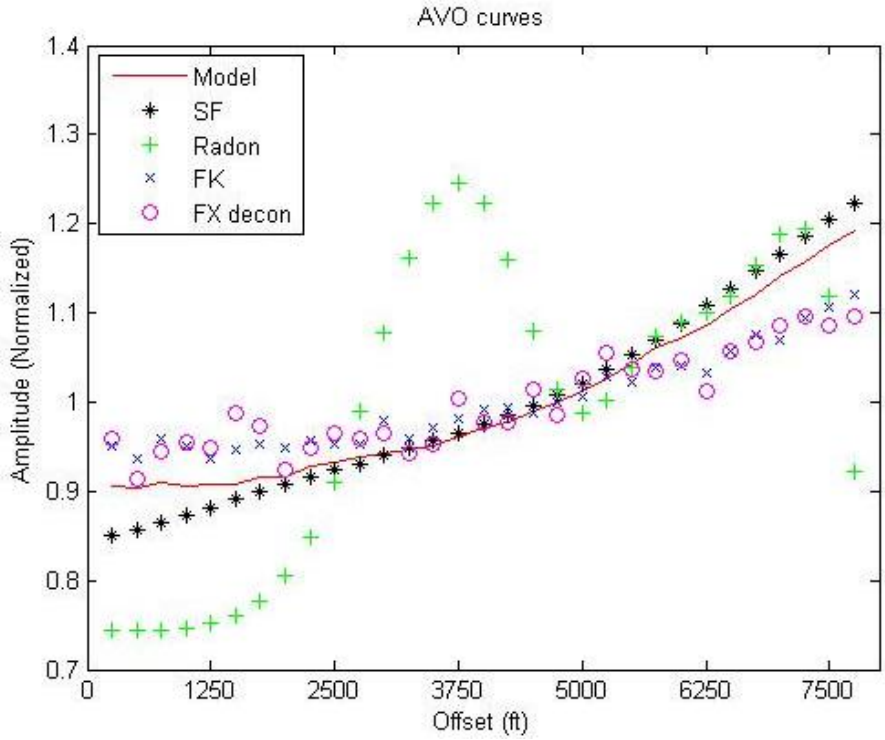

Figure 25. AVO curves for clean model, Structural Filter, Radon Filter, FK Dip Filter, and FX Decon.

The AVO curves plotted in Figure 25 confirmed that Structural Filter preserved relative reflection amplitude; Radon Filter clearly had amplitude problems at near and far offset, these amplitudes were truncated when transformed from time-moveout domain to time-space domain; FK Dip Filter fairly preserved the reflection amplitude while boosted the amplitude at near offset; and FX Decon did not preserve reflection amplitude.

5.1.3 Gradient Analysis

After AVO amplitude analysis, Gradient Analysis measured how good the amplitude at a determinate time horizon fit to a two-term Aki-Richards equation. In this study, gradient analysis was carried out at top and base of the target (around 1580 ms). Figure 26, 27, and 28 show the results of Structural Filter compared with input Clean model and noisy gathers.

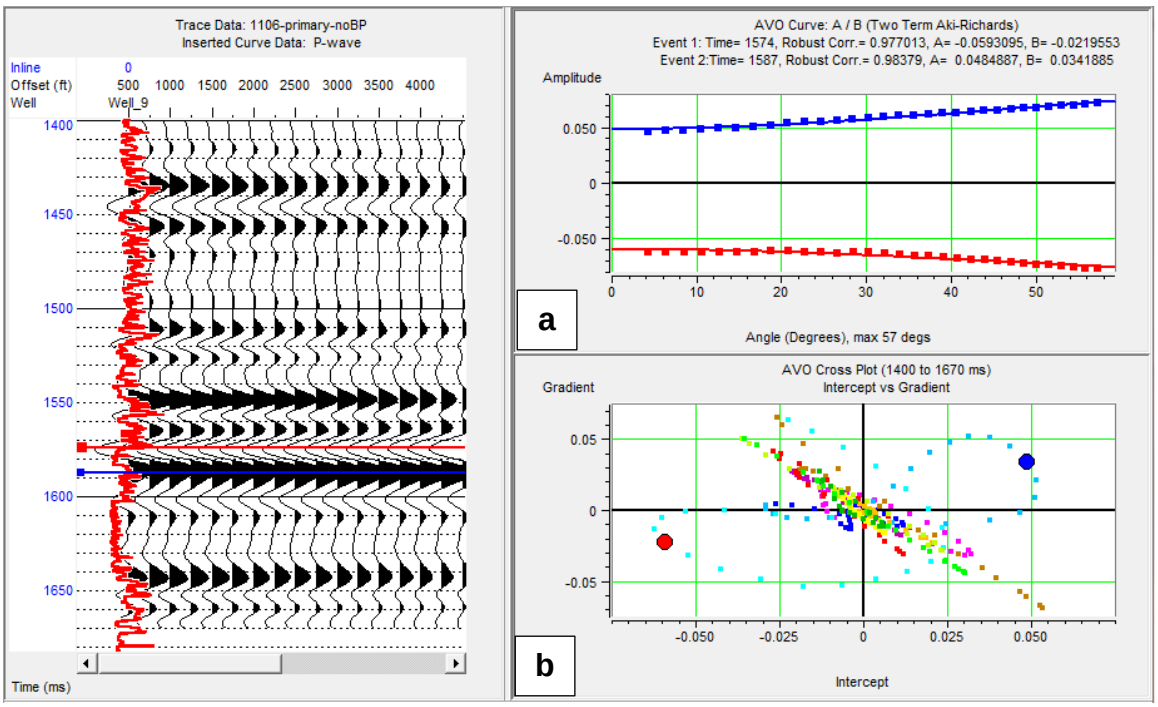

Figure 26. a) AVO Gradient analysis at top and base reservoir; b) intercept and gradient cross-plot. Clean model.

Observe that the Clean model showed amplitude increasing with offset trend in the AVO curve for top (red point) and base (blue point) of the reservoir. In AVO Cross-plot the red dot represents the top of the reservoir, it plotted into the III quadrant with negative intercept and gradient, this is an indication of class III AVO.

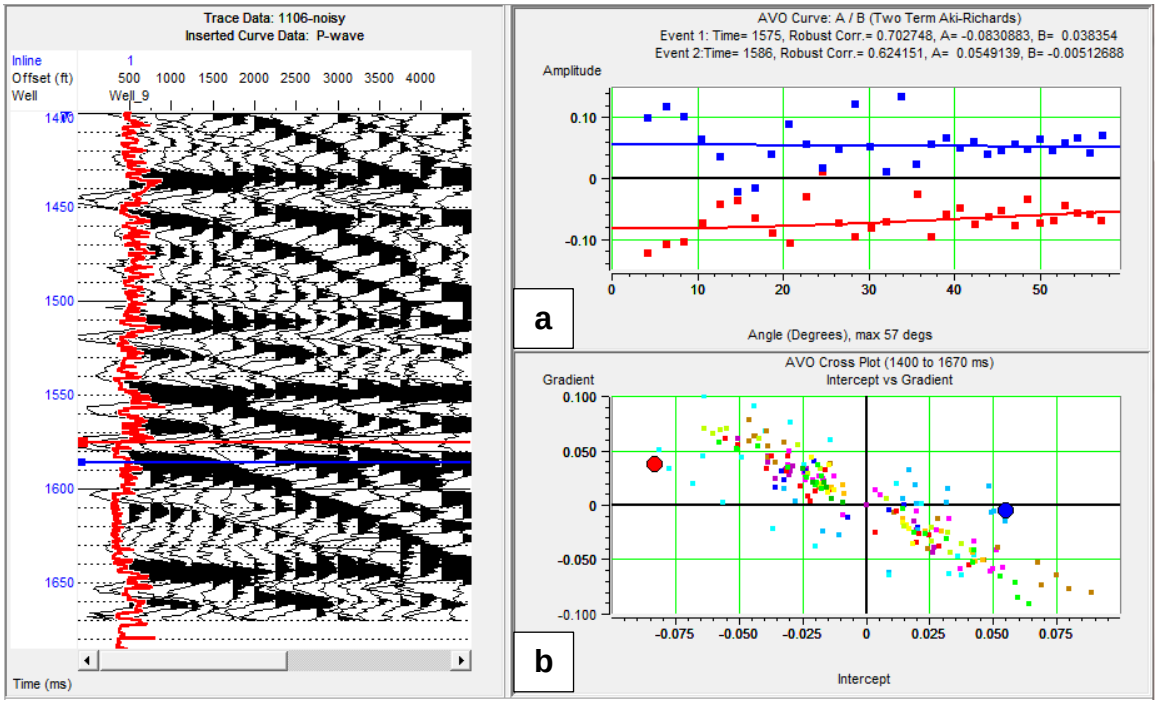

Figure 27. a) AVO Gradient analysis at top and base reservoir; b) intercept and gradient cross-plot. Noisy gather.

In the AVO curve for noisy gather, it is not possible to recognize any AVO behavior. For the AVO cross-plot, the presence of noise changed the original top base response plotting it from quadrant III to IV and made the background trend dispersive. All these effects made the amplitude interpretation impossible.

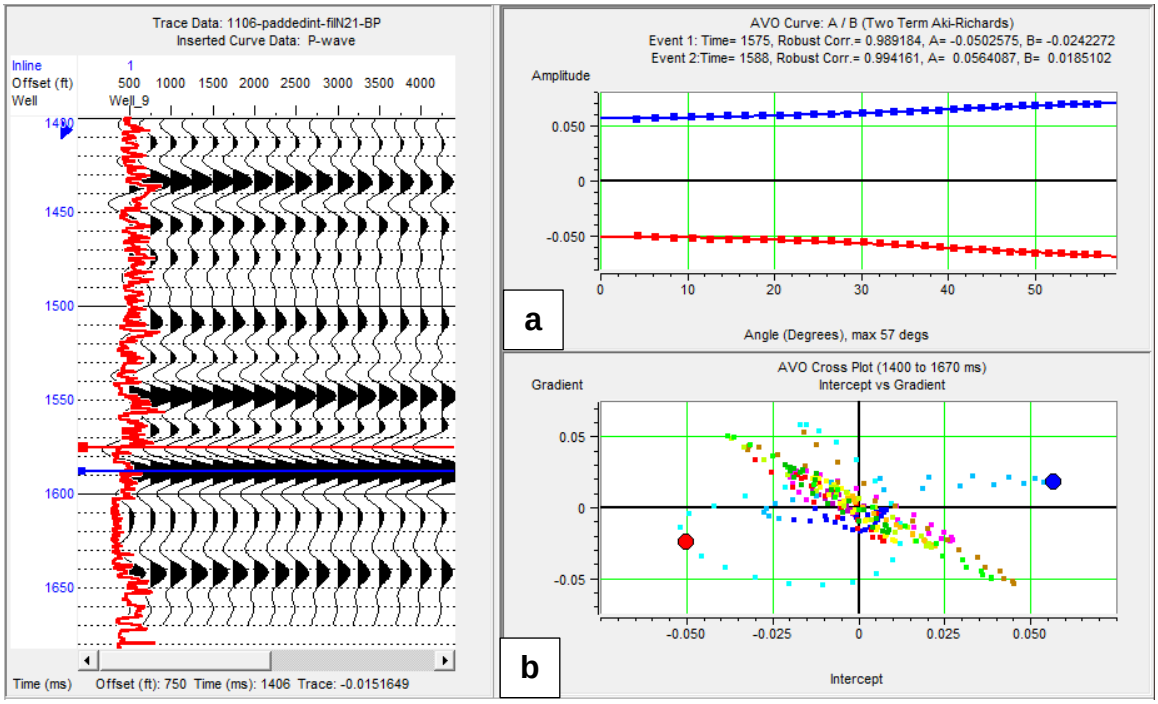

Figure 28. a) AVO Gradient analysis at top and base reservoir; b) intercept and gradient cross-plot. Structural Filter with pad intercept.

In the AVO curve, Structural Filter applied to the noisy input gather reproduced amplitude increasing with offset trend for top and base reservoir, it had an excellent fit to the two-term Aki-Richards equation giving a very high correlation factor (c=0.994). When observing the AVO intercept and gradient cross-plot, Structural Filter produced a clean and clustered background trend, this is critical when trying to differentiate deviation from the background.

When comparing Structural Filter to clean model, SF closely resembled the top and base response as in the clean model. In the AVO cross-plot, top of the reservoir plotted into the III quadrant with negative intercept and gradient, this is an indication of class III AVO.

5.2 Real Data Application

Upon confirmation of the advantages of Structural Filter in Synthetic Study, SF and other techniques are evaluated in real data. The results of real data application are presented in Gathers, Velocity Semblances, Stacks, AVO curves, Intercept and Gradient sections, and AVO cross-plots.

5.2.1 CRP Gathers

The input raw gathers are pre-stack time migrated, Common Reflection Point (CRP) gathers. They have constant offset separation of 250 ft, starting with the first offset at 500ft and ends at offset 8000ft. The reservoir zone is at about 1.58 seconds. Slight wobbles in some reflectors along the target zone can be observed (Figure 29 a). The Raw gathers has NMO correction before being processed by any filter.

Structural Filter was applied to input CRP gather with two passes, first, post-stack SF filtered common offset gathers, the filtered gathers were resorted into CMP gathers and padded intercept at front; the second pass was pre-stack Structural Filter applied to the padded intercept gathers. This two-pass process of Structural Filter is defined as cascaded SF with padded intercept (Cascaded SF Pad). For parameters used in Structural Filter and all other methods, please refer to Appendix A.

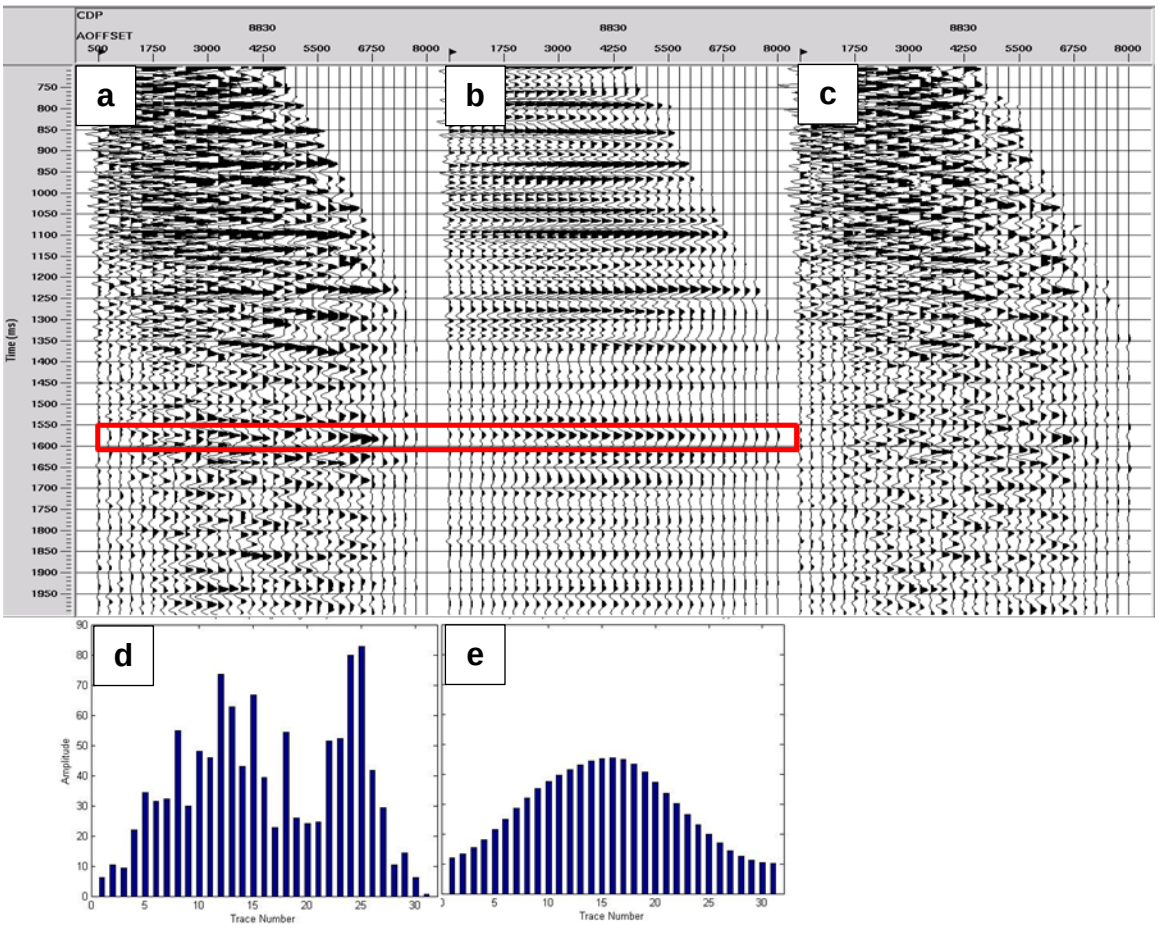

Figure 29: Cascaded SF with padded intercept, a) before and b) after Cascaded SF Pad, c) Residual. d) Amplitude plot for noisy gather and e) Amplitude plot for SF filtered gather. The amplitude plot was extracted from the target horizon (red rectangle). Signal-to-noise ratio for filtered gather after Structural Filter is SNR = 2.7427.

Cascaded SF Pad removed random noise, obtained a high signal-to-noise ratio (SNR = 2.7427), and flattened reflectors. The near offset amplitude trend is well defined or preserved, while the far amplitude seems to be reduced. This phenomenon is most likely related to post-critical angle reflections, and it will be addressed in the next subsection. Figure 30 shows Cascaded SF Pad compared with Radon Filter, FK Dip Filter, and FX Decon. Observe that Cascaded SF Pad removed random noise, produced flattened reflectors, and preserved relative amplitude.

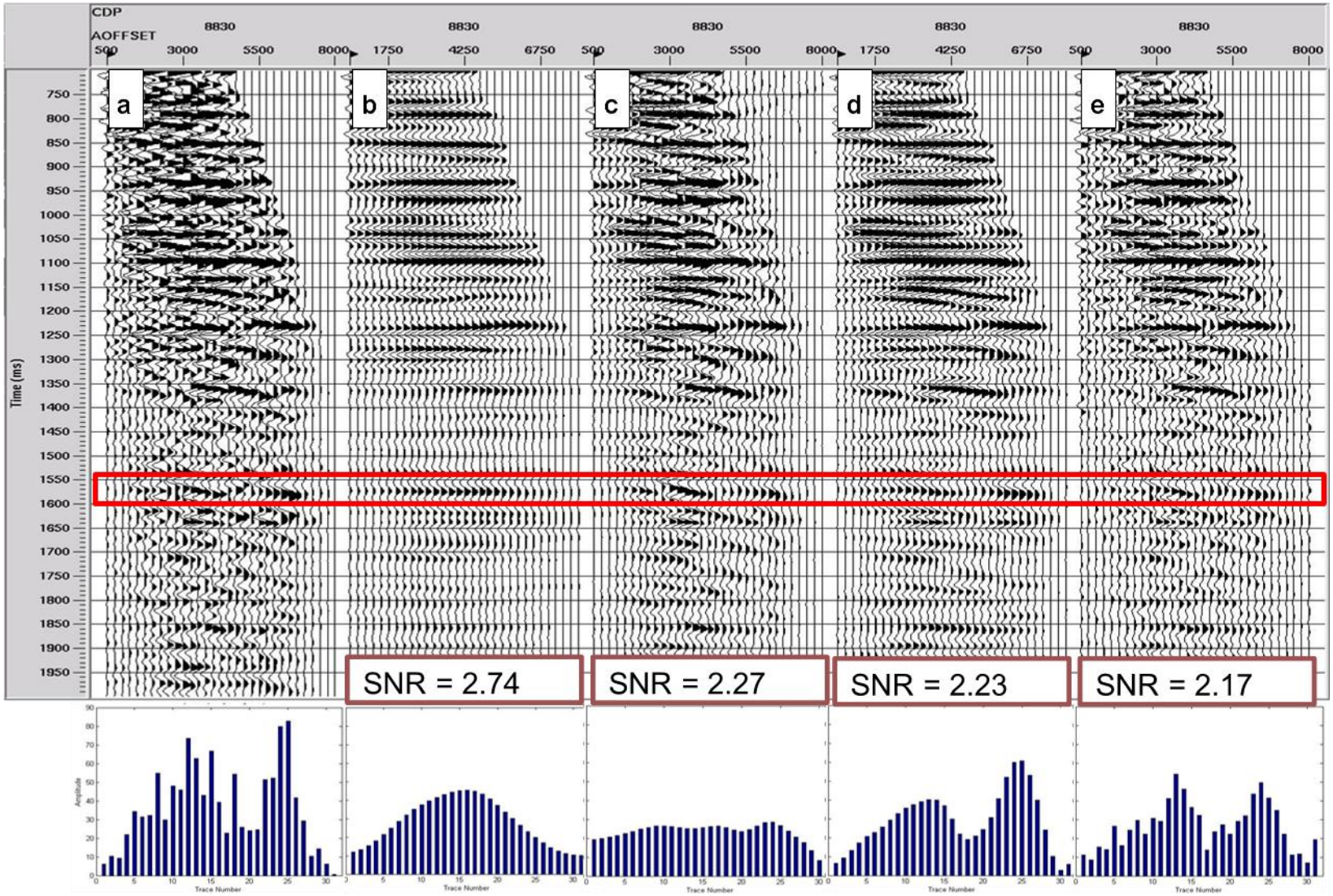

Figure 30: Raw PSTM gather a) Structural Filter b) Radon Filter c) FK Dip Filter d) and FX Decon e).

In Figure 30, all methods suppressed random noise with high efficiency. FK Dip Filter preserved the reflection amplitude at near offset but not at the far offset; Radon Filter did not preserve reflection amplitude at either near or far offset; FX Decon did not preserve reflection amplitude at all offset ranges. None of the methods gave flat reflectors, while SF flattened seismic reflectors and preserved the reflection amplitude.

5.2.2 AVO Curves

To better illustrate the effect of Structural Filter compared with the other three noise suppression techniques, Figure 31 shows the AVO curves plotted for Cascaded SF Pad with Radon Filter, FK Dip Filter, and FX Decon at the target zone.

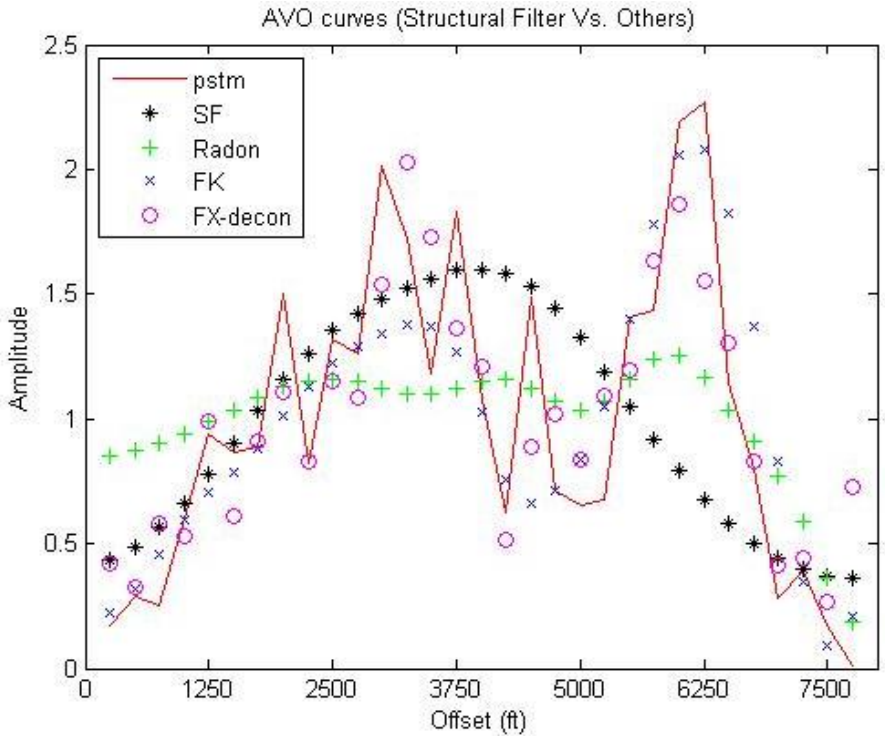

Figure 31: AVO curves for Raw PSTM gather, Structural Filter, Radon Filter, FK Dip Filter, and FX Decon.

The result curves are RMS amplitude normalized with the average value of each array. RMS amplitudes are calculated using values within a 10 ms time window around 1580 ms. Offset range are from 500 to 8000 ft (150 to 2400 m).

Observe the plotted amplitude curve as a function of offset; FX Decon has not had changed much the amplitude trend of the input raw CRP gathers and contains residual noise; FK Dip Filter trimmed near and mid offset trace's amplitude, while the far offset was practically untouched. Radon Filter diminished amplitude at near and far offset, due to the truncation effect. Structural Filter continued amplitude trend, possessed the best amplitude shaping among all the alternatives giving the same input Raw CRP gathers.

Considering the input Raw CRP gathers and output filtered gathers after different filter, notice that there is a sustainable loss of amplitude at far offset. There are many factors that could result in reflector loss, including the effects of spherical spreading, attenuation, transmission loss, signal-to-noise ratio decrease with offset, and other propagation factor (Rutherford and Williams, 1989); Thin bed tuning effect: For thin beds, such as gas sands less than 50 ft (15 m) thick, this effect results in a decrease in recorded amplitude with increasing offset. (Ostrander W. J., 1984)

Since all the factors that influence amplitude loss at far offset are outside of the scope of this study, a practical solution is to analyze the amplitude change over an angle range of 0 to 30 degrees. In such angle range the effect of amplitude loss is depreciable (Rutherford and Williams, 1989). By using table velocity (See Appendix C) an angle range of 0 to 30 degrees translates to offset range from 500 to 4000 ft (150 to 1200 m).

The RMS amplitude plot around 1580 ms, offset from 500 to 4000 ft (150 to 1200 m) is showed in Figure 32.

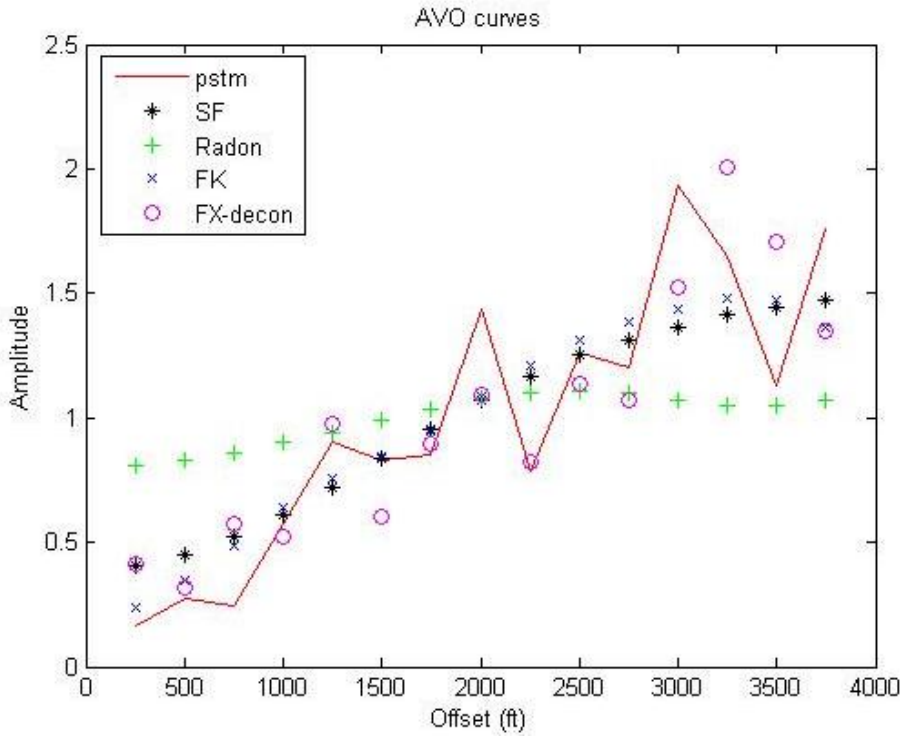

Figure 32. AVO curves for Raw PSTM gather, Structural Filter, Radon Filter, FK Dip Filter, and FX Decon. RMS amplitude plot around 1580 ms in an offset range from 500 to 4000 ft (150 to 1200 m).

When compared the RMS amplitude plot in an offset range from 500 to 4000 ft (150 to 1200 m), Structural Filter and FK Dip Filter showed a clear amplitude increase with offset AVO anomaly, while Radon Filter and FX Decon did not show an AVO anomaly. A closed analysis suggested that SF is even better than FK because the later reduces reflection amplitude at near offset, which is undesired in AVO analysis.

5.2.3 Velocity Analysis and Stacks

Velocity analysis and stacks are important in seismic study, because many processes depend on a well formulated velocity field, such as migration. This section shows velocity semblance and stacks comparing input raw data and SF filtered data (Figure 33 and 34), the idea is to see how velocity and stacks improved after Structural Filter was applied.

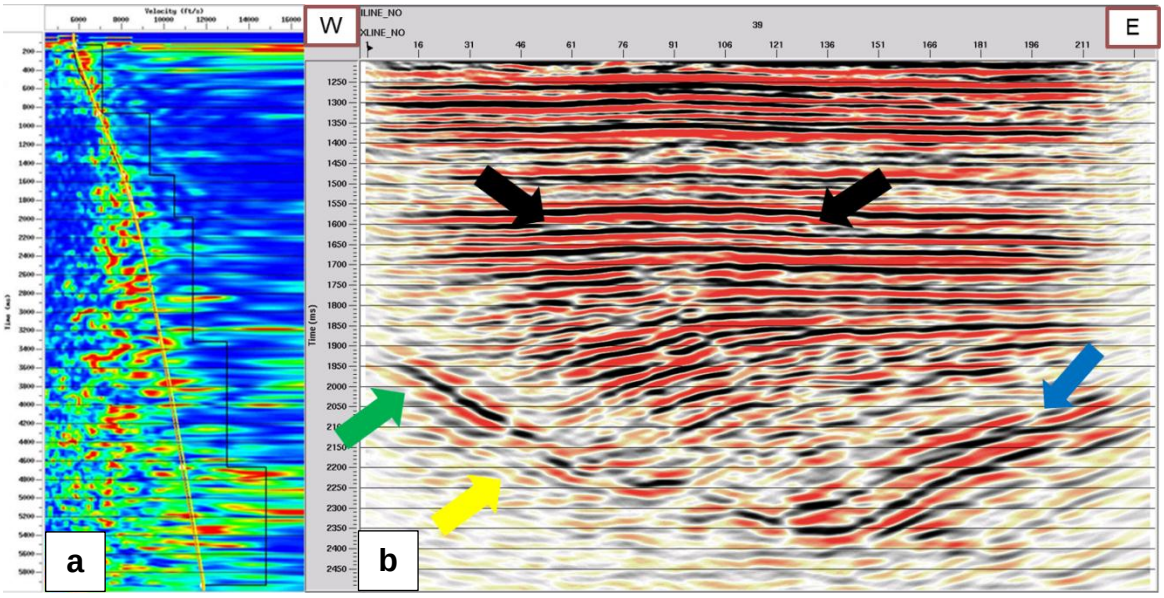

Figure 33: a) Velocity semblance b) Stack; raw PSTM gather.

Observe the velocity semblances before and after Structural Filter, the input raw data is very noisy with apparent multiple, the peak energy in the semblance is not concentrated (Figure 33 a); SF produced a cleaner semblance, with apparent multiple attenuated, and the peak energy is much more concentrated (Figure 34 a). Using this improved velocity, stack data from SF filtered gather was created. Figure 33-b and Figure 34-b illustrate the input raw stack and stack after filter applied.

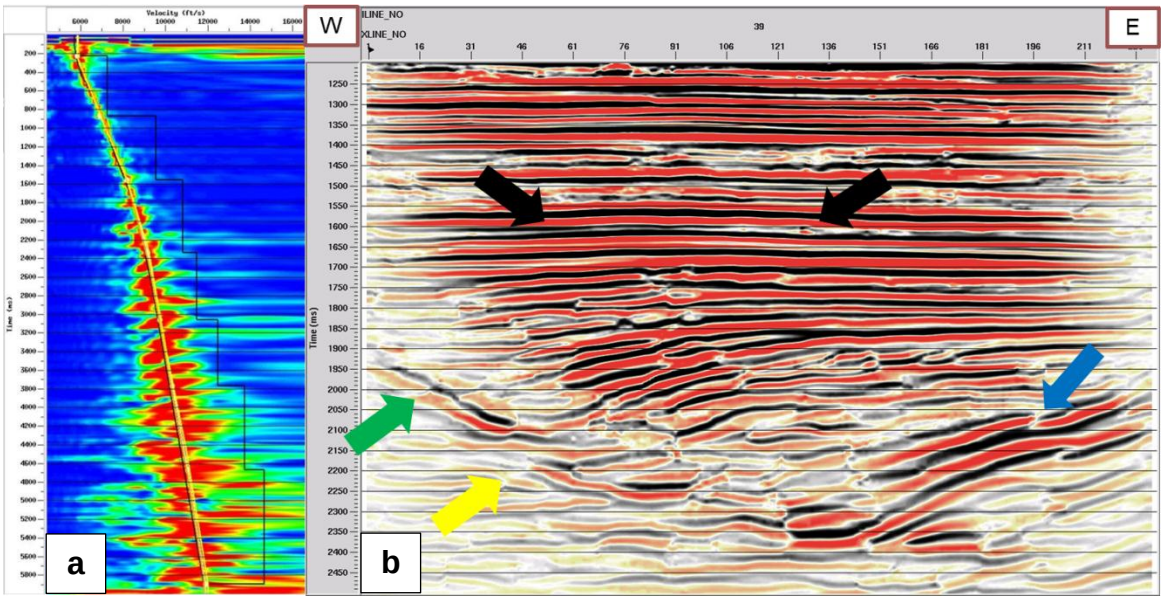

Figure 34. a) Velocity semblance b) Stack; Structural Filter.

In Figure 33-b the raw stack presented non-flat reflector with poor continuity and faults that are not well defined. When observing the stack section from Figure 34-b, SF flattened reflectors and made events more continuous (black arrows), it not only preserved faults but also better defined them (green, yellow, and blue arrow).

To further examine the advantage of Structural Filter and compare the results with other methods, the AVO Intercept and Gradient Analysis was done. The following two subsections show Intercept and Gradient section and cross-plot.

5.2.4 Intercept and Gradient Sections

In order to determinate whether Structural Filter and other methods are AVO compliant noise suppression methods, the AVO Intercept and Gradient sections were extracted from raw and filtered data. These sections are presented in time slices (Figure 35 to 39), which were produced at top of the reservoir (about 1580 ms).

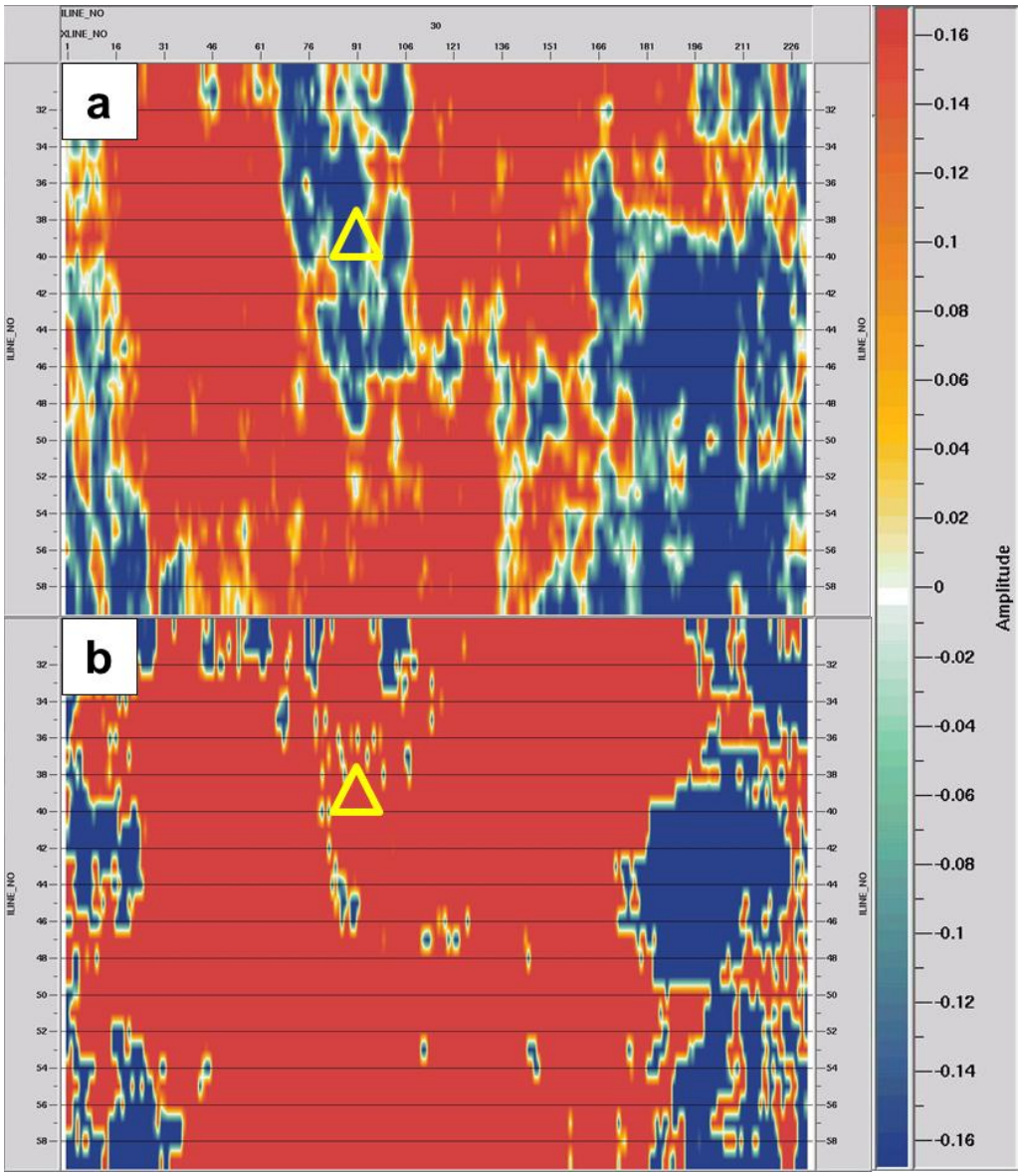

Figure 35. Time slices for raw CRP Gathers. a) Intercept, b) Gradient; yellow triangle indicates the well location.

The time slices for intercept and gradient section extracted from the raw CRP gathers showed noisy intercept and gradient section. The target seems to have negative intercept and positive gradient.

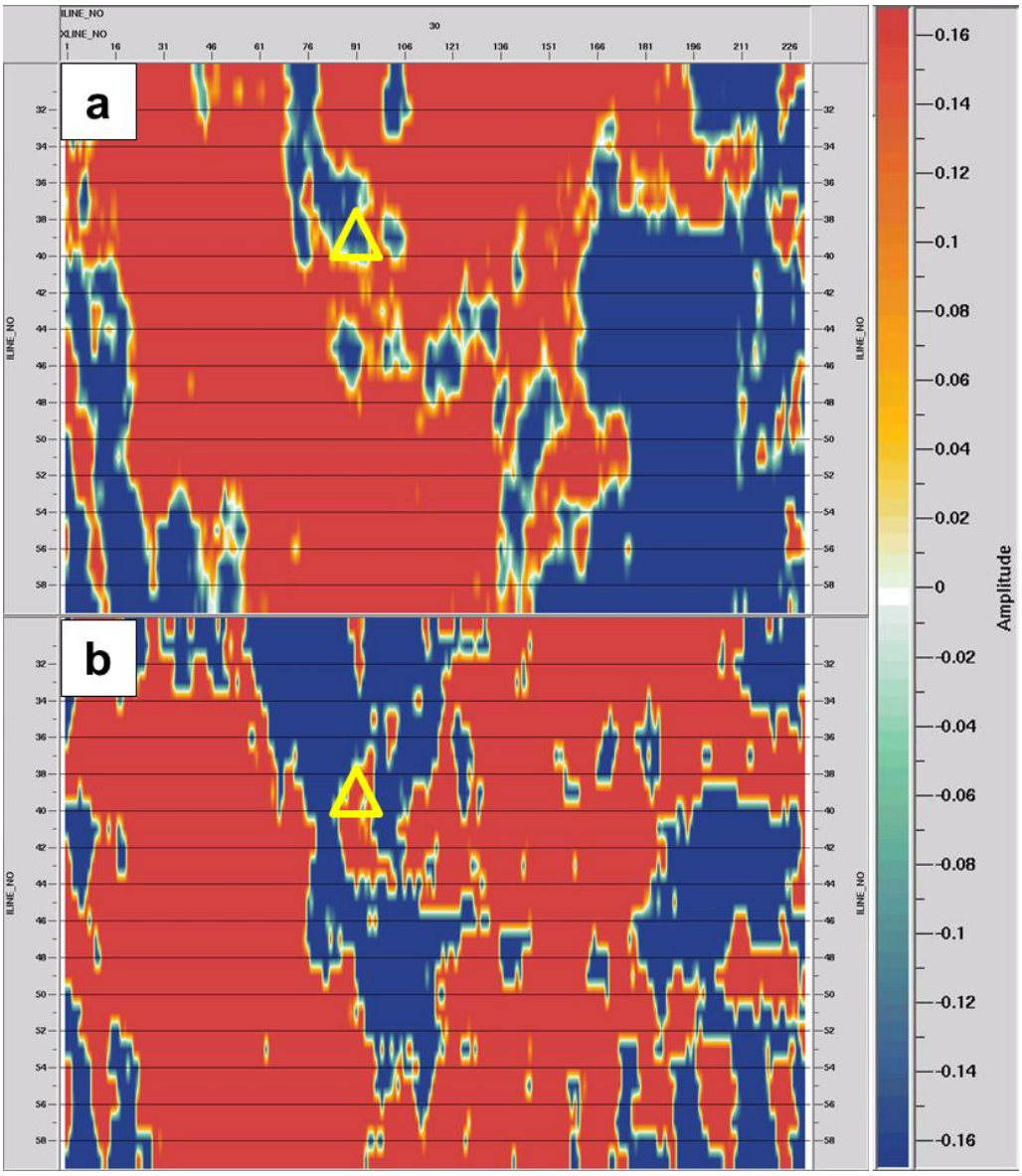

Figure 36. Time slices for Radon Filter. a) Intercept, b) Gradient; yellow triangle indicates the well location.

The time slices for intercept and gradient section extracted from gathers after Radon Filter showed improved intercept and gradient section, less noisy than the raw data. The target seems to have negative intercept and negative gradient. Nevertheless, it is difficult to determine because in both intercept and gradient section the well locations are surrounded by amplitude of the other sign.

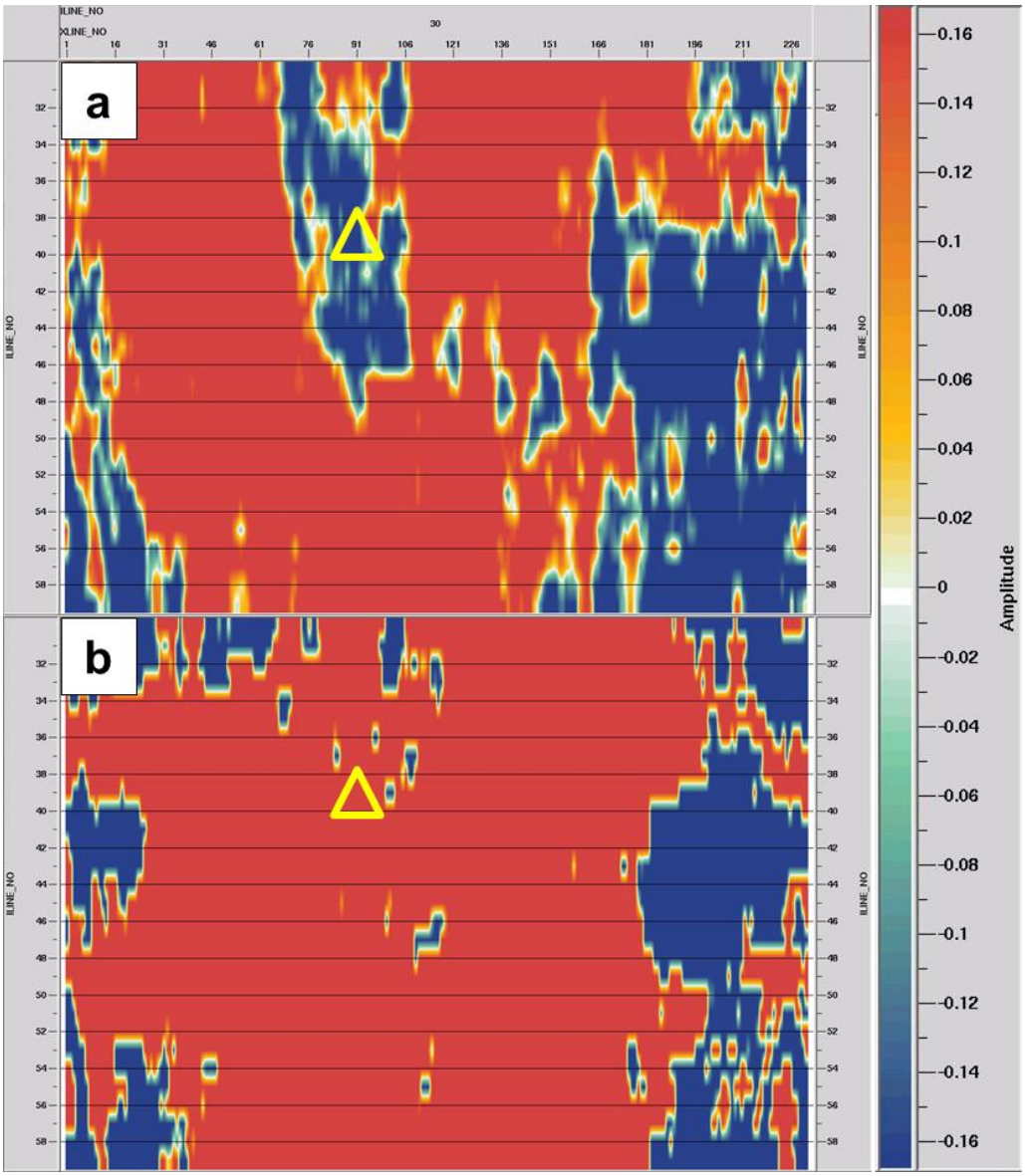

Figure 37. Time slices for FK Dip Filter. a) Intercept, b) Gradient; yellow triangle indicates the well location.

The time slices for intercept and gradient section extracted from gathers after FK Dip Filter showed presence of residual noise, it offered no significant improvement over the raw data. The target seems to have negative intercept and positive gradient.

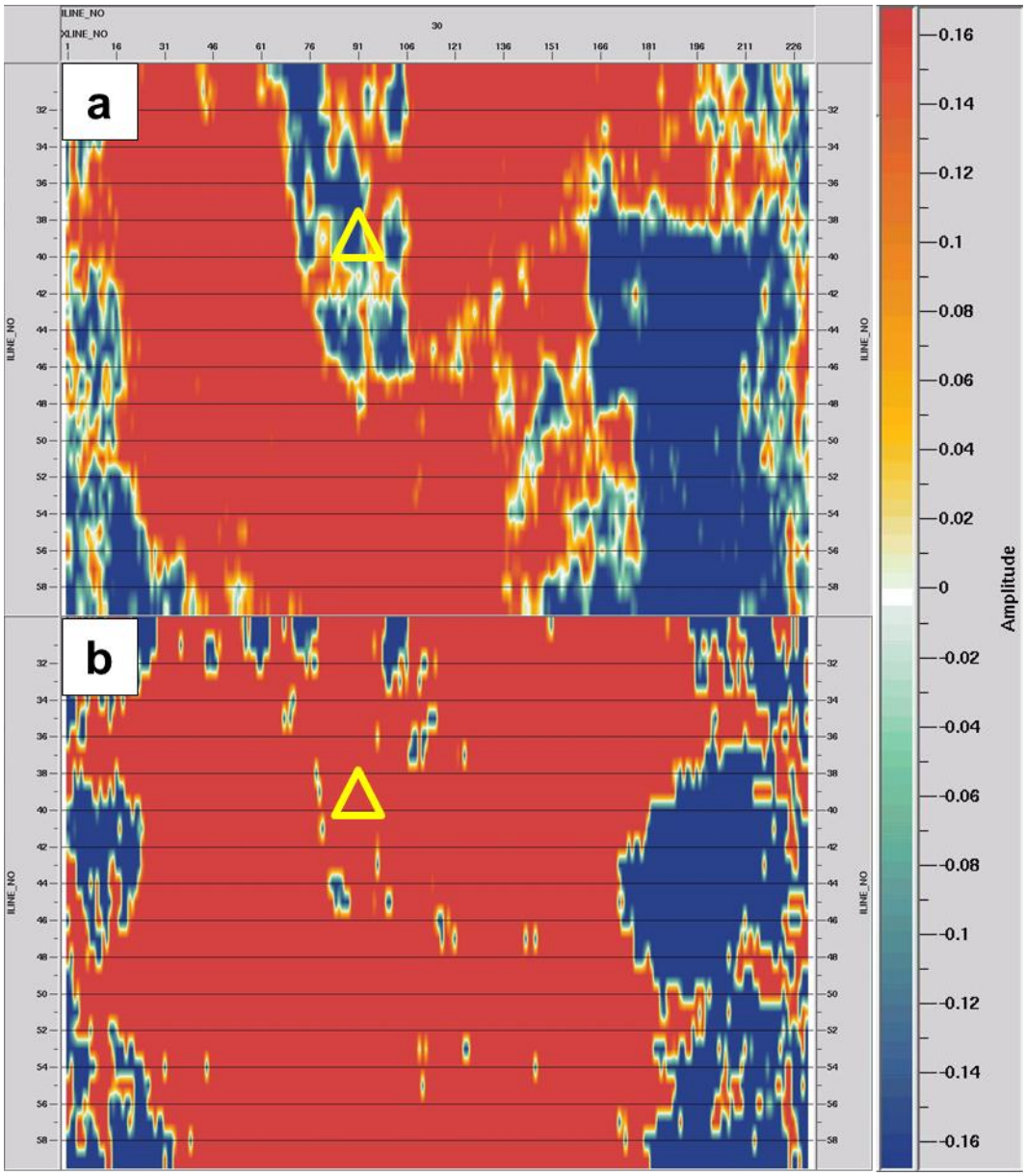

Figure 38. Time slices for FX Decon. a) Intercept, b) Gradient; yellow triangle indicates the well location.

The time slices for intercept and gradient section extracted from gathers after FX Decon also showed no significant improvement over the raw data. They displayed negative intercept and positive gradient at the target.

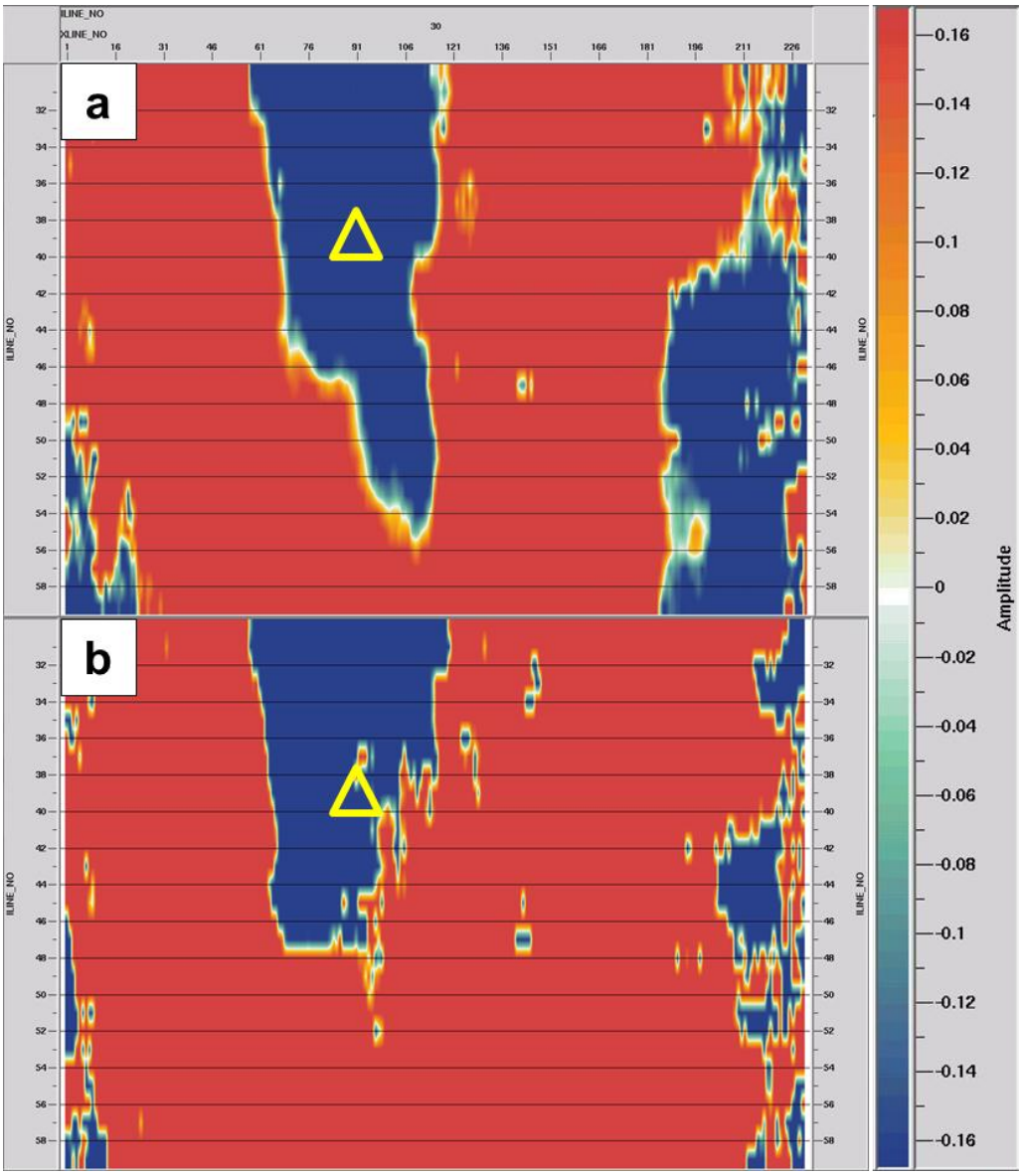

Figure 39. Time slices for Structural Filter. a) Intercept, b) Gradient; yellow triangle indicates the well location.

The time slices for intercept and gradient section extracted from gathers after Structural Filter showed very clean intercept and gradient, substantial improvement from the raw data.

Clearly the target has a negative intercept and gradient. The negative intercept and gradient potentially indicate a class III avo. Imaging a negative amplitude anomaly that is coming out from a positive one needs to be detected. SF is the proper tool to reveal the anomaly and make it visible to interpreters.

When compare the intercept and gradient sections for all four methods, Structural Filter is superior to others. The time slices for intercept and gradient section extracted from gathers after SF showed less affected by noise, which helped greatly to define AVO class.

To further determine the advantage of Structural Filter over other methods, AVO Intercept and Gradient Analysis was done. The results are showed in the next subsection.

5.2.5 AVO Cross-plots

In the Intercept and Gradient cross-plots shown in Figure 40-44, the black polygon in Seismic Section, marked by letter a, and High Gradient Anomaly, marked by letter b, represent the reservoir zone. Within the black polygon, the center CDP number is 8830, where the production well (Well-9) is located; the green polygons in both Seismic Section and Gradient Anomaly represent the non-production zone, which serve to define the background shale. Additionally, there are three polygons in the cross-plot area (letter c): red polygon represents top of the reservoir, blue polygon represents base of the reservoir, and gray polygon represents background trend.

The AVO cross-plots were created by first defining two polygons in the seismic section, the black polygon, which is the production area where the well symbol; the green polygon, which represent the non-production zone. Next, the amplitude values defined by the polygon are plotted into the AVO cross-plot area, the non-production green point form the background shale and black point represent deviation associated with top base of reservoir. In the cross-plot, two polygons were picked to delimit top and base reservoir. Finally, the top and base response was projected from cross-plot to the gradient anomaly plot.

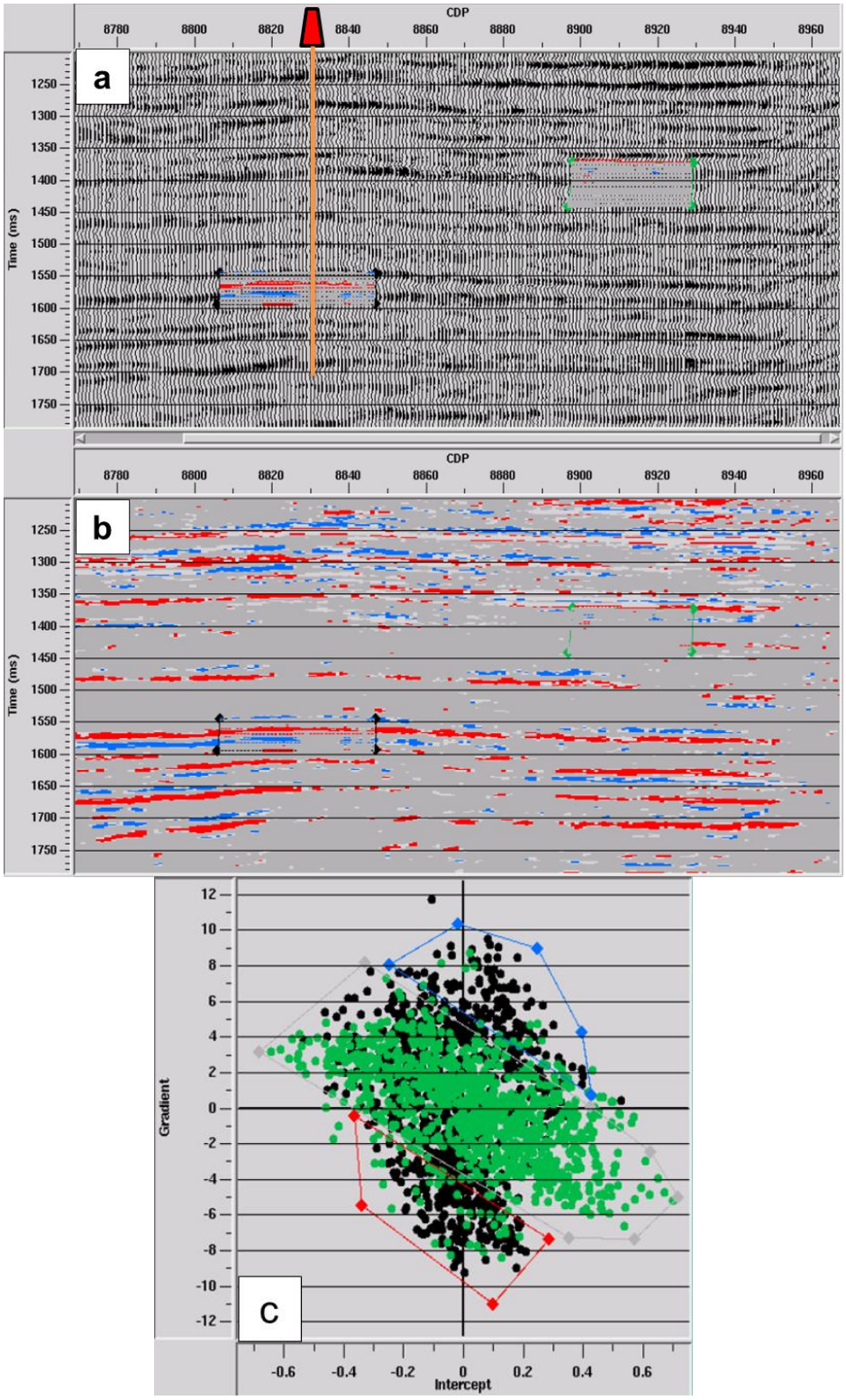

Figure 40. AVO cross-plot for raw PSTM gather. a) Seismic section. b) High gradient anomaly. c) Intercept and Gradient Cross-plot.

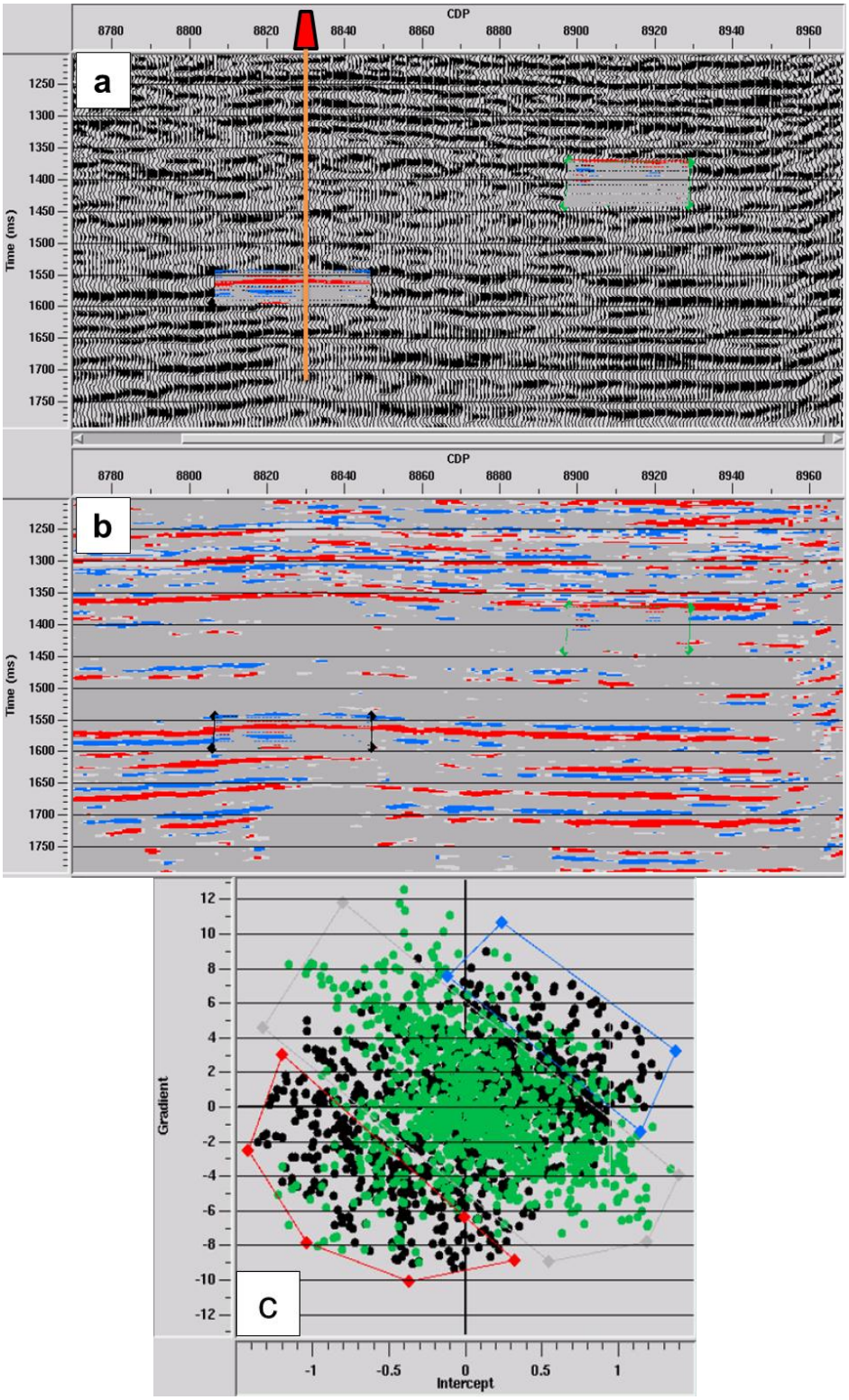

Figure 41: AVO cross-plot for Radon Filter. a) Seismic section. b) High gradient anomaly. c) Intercept and Gradient Cross-plot.

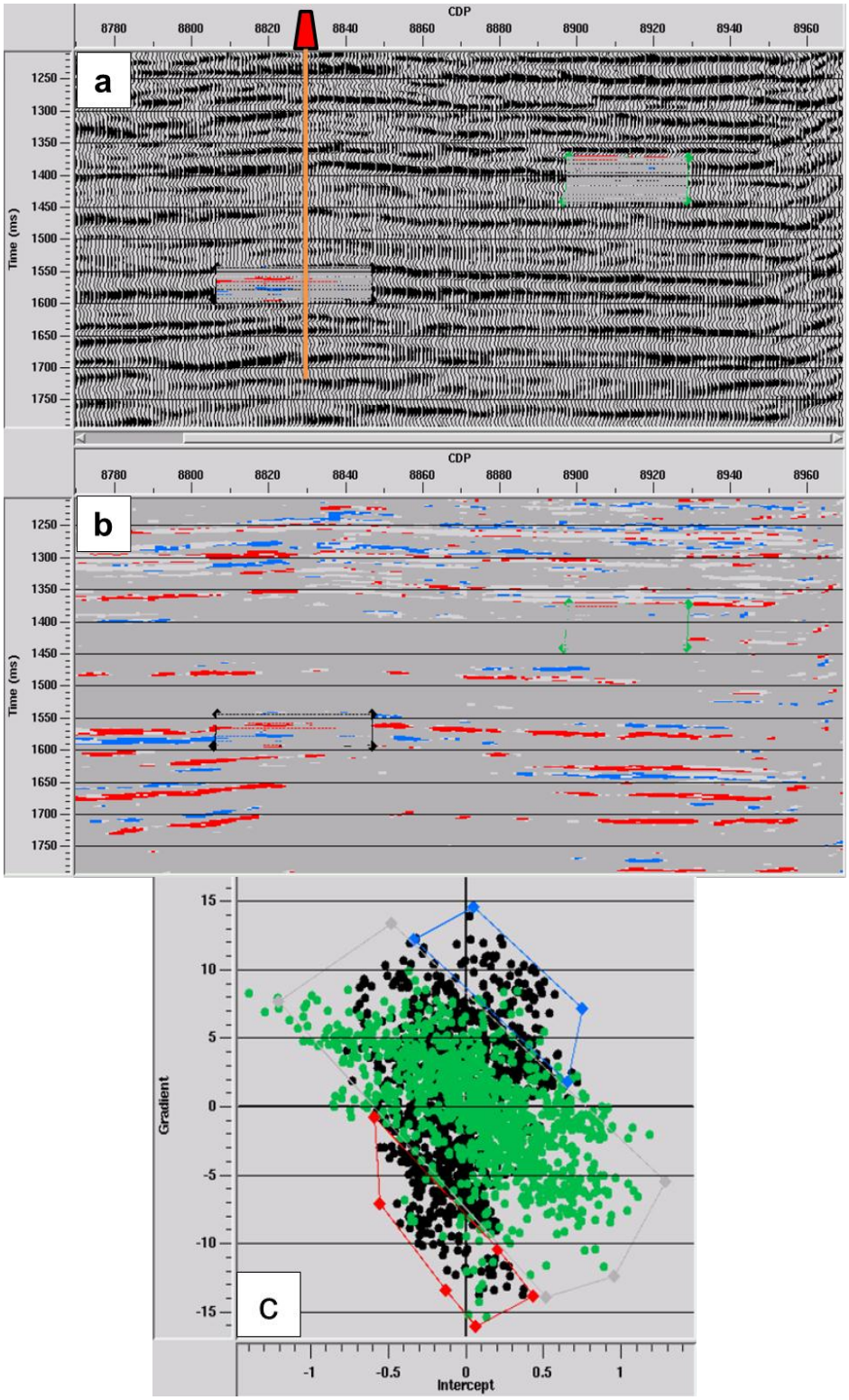

Figure 42. AVO cross-plot for FK Dip Filter . a) Seismic section. b) High gradient anomaly. c) Intercept and Gradient Cross-plot.

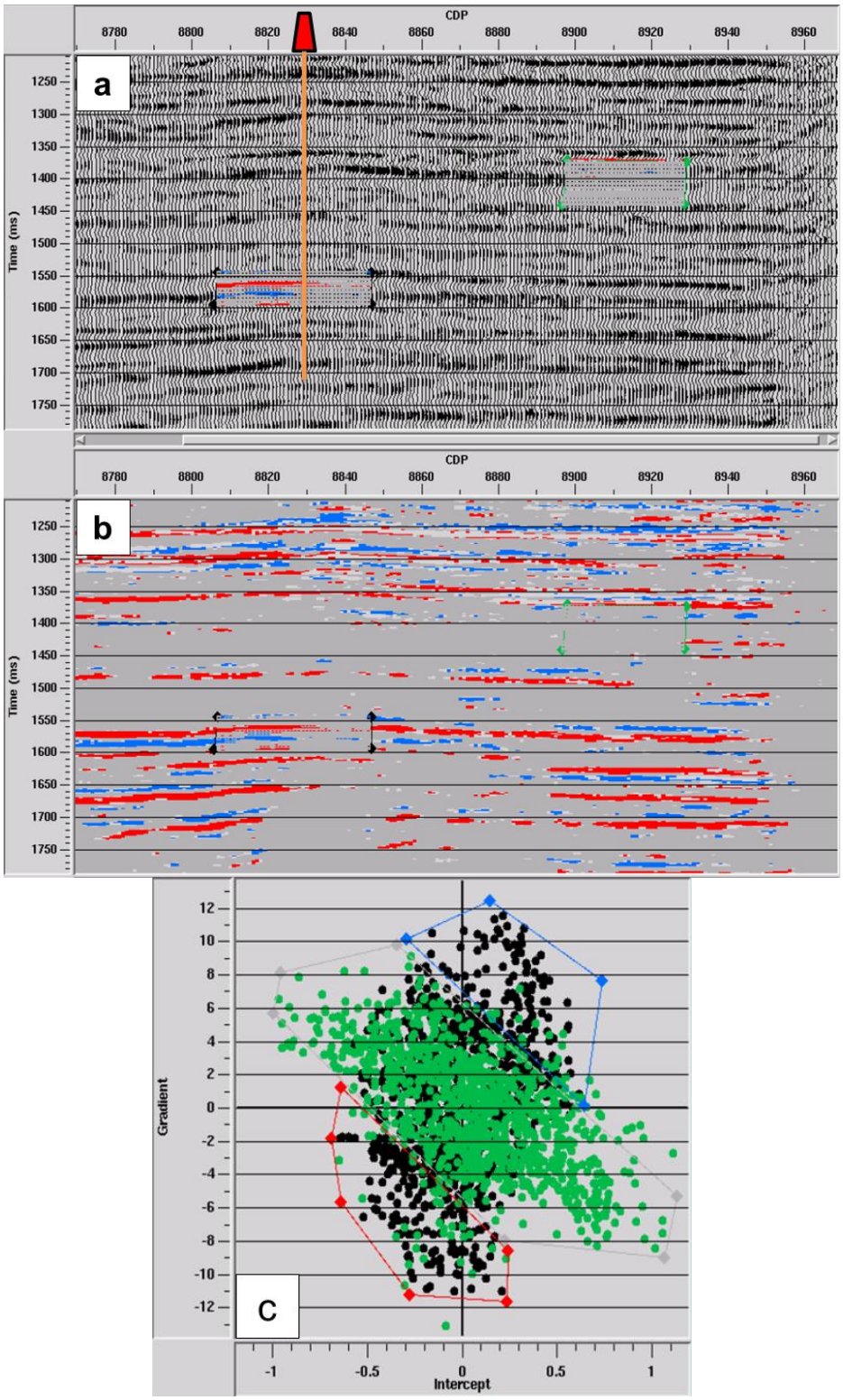

Figure 43. AVO cross-plot for FX Decon. a) Seismic section. b) High gradient anomaly. c) Intercept and Gradient Cross-plot.

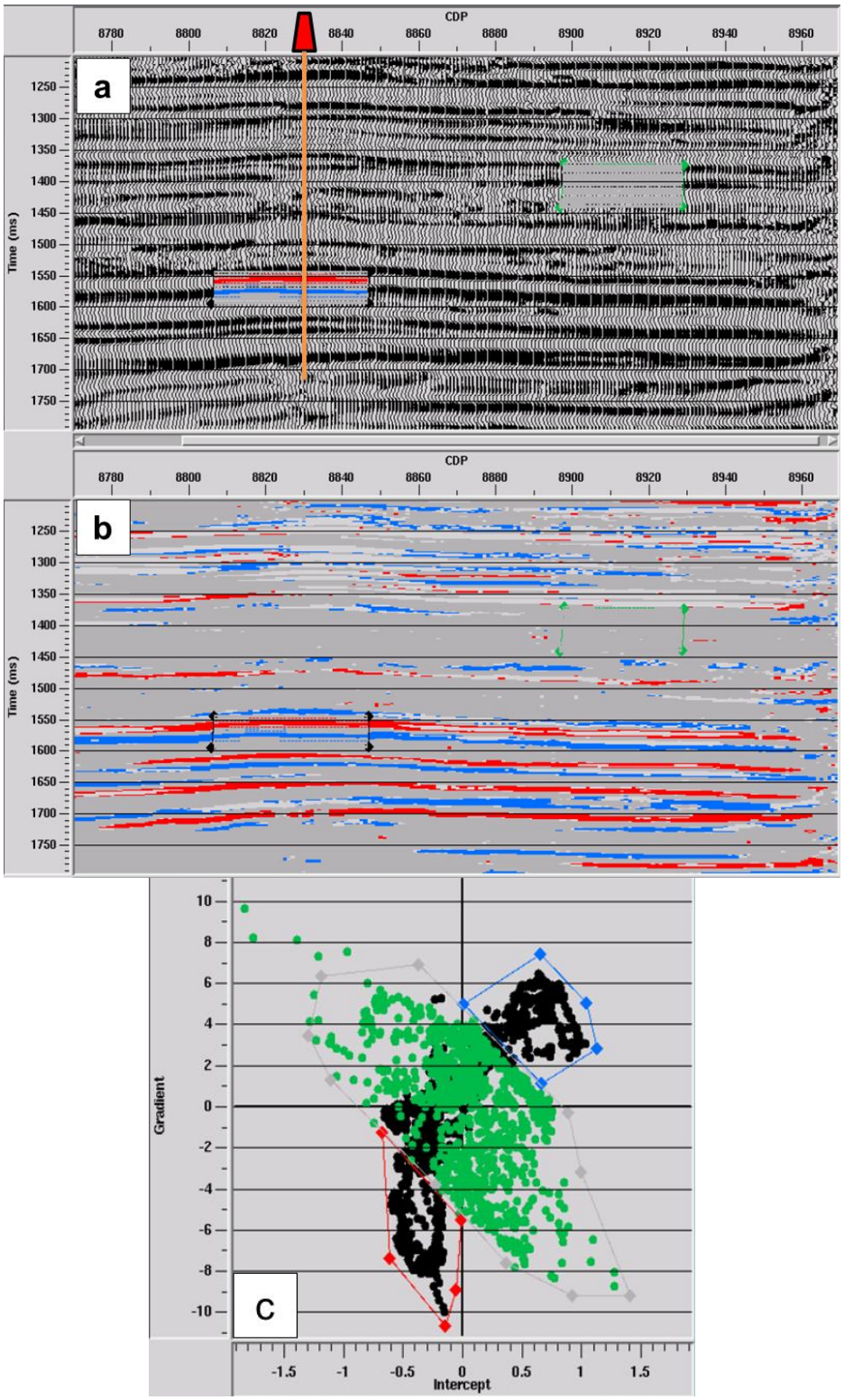

Figure 44. AVO cross-plot for Structural Filter. a) Seismic section. b) High gradient anomaly. c) Intercept and Gradient cross-plot.

Studying the initial cross-plot for Raw CRP gather in Figure 40, the noise background trend made it difficult to differentiate top and base reservoir. In area b, where plotted high gradient anomaly, the top and base reservoir cannot be seen clearly with continuity. The same tendency can be observed in the cross-plot on data after Radon Filter, FK Dip Filter, and FX Decon. Radon Filter made the background trend even noisier to differentiate top and base of the reservoir (Figure 41). FK Dip Filter suppressed noise in the background trend but weakened the deviation response from the background, resulting in little improvement to define high gradient anomaly (Figure 42). Data after FX Decon showed mostly no difference from the input raw gather, this method offered no improvement in AVO analysis (Figure 43).

When examine the Intercept and Gradient cross-plot in Figure 44, it was easy to differentiate deviation (black dots) from background (green dots), because the later was well clustered. Structural Filter better defined the background by suppressing random noise and it precisely estimated the gradient amplitude by using the pre-padded intercept information extracted from the same data. This result again confirmed that Structural Filter preserved relative reflection amplitude at near and far offset, and it can significantly improve AVO analysis.

Chapter 6

Conclusion

Structural Filter (SF) has been proved to be an AVO compliant pre-stack noise suppression technique. SF helped to refine seismic reflectors continuity and conserved stratigraphic features such as faults. It preserved relative reflection amplitude, suppressed random noise, enhanced velocity analysis, and improved AVO intercept and gradient sections and cross-plots.

Post-stack SF should be applied to Common Offset Gathers with CMP stack from the same data as a pilot stack. Because the stack section provides local dip information of the data, Post-stack SF is misleading when applied to common offset gathers without a pilot stack; In CO domain, SF presented a tradeoff between fault detection and noise reduction; this effect can be adjusted by choosing properly the Fault Detection Threshold.

Pre-stack Structural Filter is applied directly in the CMP Gathers with the local dip information calculated from the same gathers. In this domain SF presented border effect, which was corrected by using padded AVO intercept. The automated extraction of AVO intercept from data and the use of this information in filtering process become the key feature of Structural Filter.

The use of Structural Filter in Stratton Field data has proved that the best workflow is the cascaded SF with padded intercept (Cascaded SF Pad). The Cascaded SF Pad was superior to Radon Filter, FK Dip Filter, and FX Decon in overall

performance, because it preserved relative amplitude, removed random noise, flattened seismic reflectors, and enhanced stratigraphic features such as faults and fractures.

In addition, SF applied to pre-stack time migrated gathers obtained velocity semblance with apparent multiples attenuated. With the improved velocity, better stack sections are produced for structure identification and interpretation.

Using the conditioned CRP gathers in AVO analysis, it was possible to improve intercept and gradient sections and cross-plots. The intercept and gradient sections showed negative intercept and negative gradient for top reservoir sand, indicating an AVO class III response, which is AVO anomaly associated with amplitude increase with offset; AVO cross-plots showed that Structural Filter defined a cleaner and clustered background trend which allowed us to better differentiate deviations associated with top and base of the reservoir.

The application of Structural Filter in synthetic and real seismic data has proved that SF is a great tool for AVO data conditioning, and the use of this noise suppression technique in Stratton Field data for AVO Analysis may potentially help to find new prospect for exploitation and production in Gulf Coast Basin.

References

Abbad B., B. Ursin, and M.J. Porsani, 2006 A fast, modified parabolic Radon transform: Geophysics,Vol. 76, No. 1 2011, pp. 11–24

Abma, R. and J. Claerbout, 1997, Lateral prediction for noise attenuation by t-x and f-x techniques: Stanford Exploration Project, Report 79, pp. 15-35

Canales L.L., 1984, Random noise reduction: SEG Expanded Abstracts, Vol. 3 pp. 525-527 (1984)

Castagna, J.P., 2001, AVO analysis, CSEG Recorder, pp. 29-34.

Castagna, J.P., 2001, Recent advances in seismic lithologic analysis: Geophysics Vol. 66, No.1, pp. 42-46.

Castagna, J.P., H. W. Swanz, and D. J. Foster 1998, Framework for AVO gradient and intercept interpretation: Geophysics Vol. 63, No.3, pp. 948-956.

Chopra S. and K. Marfurt, 2008, Emerging and future trends in seismic attributes: The Leading Edge, Mar 2008. pp. 298-318.

Christopher P. R. 2000, Effective AVO crossplot modeling: A tutorial: Geophysics. Vol. 65, No. 3; pp. 700-711.

Eichkitz C. G., J. Amtmann and M. G. Schreilechner 2012. Enhanced coherence attribute imaging by structurally oriented filtering: First Break, Vol. 30. pp. 75-81.

Fehmers, G. and C. Hocker, 2003, Fast structural interpretation with structure-oriented filtering: Geophysics, Vol. 68, No. 4. pp. 1286–1293

Gulunay, N., 1986, FX Decon and complex wiener prediction filter: 56th Annual Internat. Mtg., SEG Expanded Abstracts, Session: POS 2.10.

Hall, M., 2007, Smooth operator: Smoothing seismic interpretations and attributes: The Leading Edge, January 2007 pp. 16-20.

Liu, Y., C. Liu and D. Wang, 2009, A 1-D time-varying median filter for seismic random, spike-like noise elimination: Geophysics, Vol. 74, pp.17-24.

Mavko G., T. Mukerji and J. Dvorkin, 2009, The Rock Physics Handbook: Tools for

Seismic Analysis of Porous Media. 2nd Edition, pp 226-228.

Meinardus, H. A., R.D. Martinez, R. Sanchez, and J. Cisneros., A 3D Land Processing Sequence for AVO Purposes Using Noisy Seismic Data: A Case History. Seismic Processing 4: In Search of Imaging, pp. 1127-1130.

Nam N. and L. Fink, 2008, From Angle Stacks to Fluid and Lithology Enhanced Stacks: International Conference & Exposition on Petroleum Geophysics, HYDERABAD 2008, pp. 41-46.

Nowak E.J. and M.G. Imhof 2006, Amplitude preservation of radon-based multiple-removal filters: Geophysics, Vol. 71, No. 5 pp. 123–126.

Ostrander, W. J., 1984, Plane-wave reflection coefficients for gas sands at nonnormal angles of incidence: Geophysics, Vol. 49, No. 10; pp. 1637-1648.

Ogiesoba O. C., W. Wright, F. Wang, M. V. Popini, M. P. Franco, A. T. Lourenco, and G. B. D. da Silva 2011, Seismic conditioning and attenuation of high-angle coherent noise in a mixed carbonate and siliciclastic setting, Campos Basin, offshore Brazil: A case study: Geophysics. Vol. 76, No. 5, pp. 199–212.

Raymond A. L., B. A. Hardage, R. Edson, and V. Pendleton, 1994. 3-D Seismic Well Log Data Set Fluvial Reservoir Systems-Stratton Field, South Texas: BEG report, pp 1-30.

Robert E. M., J.P. Nicot, A. H. Chowdhury, A. R. Dutton, and S. Kalaswad 2006, Please Pass the Salt: Using Oil Fields for the Disposal of Concentrate from Desalination Plants: Texas Water Development Board Report 366. pp. 60, 68, 84-88.

Russell, B., D. Hampson and J. Chun, 1990, Noise elimination and the Radon transform Part 1 and Part 2. Geophysics: The Leading Edge of Exploration; pp. 18-23, 31-37.

Rutherford, S.R. and R. H. Williams, 1989, Amplitude-versus-offset variations in gas sands: Geophysics. Vol. 54, No. 6; pp. 680-688.

Simmons J.L. Jr. and M.M. Backus, 1994, AVO modeling and the locally converted shear wave: Geophysics. Vol. 59, No. 9; pp. 1237-1248.

Singleton, S., 2009, The effects of seismic data conditioning on pre-stack simultaneous impedance inversion: The Leading Edge, June 2009. pp. 260-267.

Smith J. H., 2011, Pseudo-sonics, synthetics and the lay of the land: SIPES February 2011, pp. 31-33.

Steven J.S. and G.W. Timothy, 1994, Geothermal and Heavy-Oil Resources in Texas Topical Report: BEG Report, pp. 6.

Swisi, A. and I. Morozov, 2010, Inversion of 3D Seismic Dataset, post and pre-stack attribute analysis of Blackfoot 3D Seismic Dataset. pp. 1-2.

Vaseghi, S. V., 2008, Advanced digital signal processing and noise reduction. J. Wiley & Sons, Ltd, UK. 4th Edition. p.p. 35-50

Yilmaz, O., 2001, Processing, Inversion, and Interpretation of Seismic Data: Society of Exploration Geophysics. Volume I, p.p. 898-920.

Yu G., 1985, Offset-amplitude variation and controlled-amplitude processing: Geophysics, Vol. 50, No. 12, pp. 2697-2708

Appendix A

Synthetic Study

Post-stack Structural Filter, Post-stack SF along common offset gather only. Nx=21.

Pre-stack Structural Filter, Pre-stack SF across raw cdp gather only, Nf=21

Pre-stack Structural Filter with pad intercept, Pre-stack SF across cdp gather with pad intercept, Nf=21

Radon Filter, across cdp gather combining primary pass and multiple subtract. P=210

FK Dip Filter, Simple pass across raw cdp gather. (Arbitrary polygon)

FX Decon, Simple pass across raw cdp gather. (Wiener Levinson, f=250)

Real Data Application

Post-stack Structural Filter, Post-stack SF along common offset raw gather only. Nx=21.

Pre-stack Structural Filter, Pre-stack SF across raw cdp gather only, Nf=11

Pre-stack Structural Filter with pad intercept, Pre-stack SF across raw cdp gather with pad intercept, Nf=11

Post-Pre stack cascaded Structural Filter, Pre-stack SF applied to Post-stack SF filtered common offset gather with pad intercept. Nf=11

Radon Filter, across raw cdp gather, primary pass plus multiple subtract. P=230

FK Dip Filter, Simple pass across raw cdp gather. (Arbitrary polygon)

FX Decon, Simple pass across raw cdp gather. (Wiener Levinson, f=250)

Appendix B

AVO Intercept

AVO intercept is an AVO attribute that represent the zero offset incidence reflection amplitude (Figure 45). The idea of padding intercept in front of gather is to give the correct amplitude value to SF, knowing that amplitude smoothing within SF filtering window is done by Median Filter. By interpolating amplitude from the intercept trace with the amplitude in the original gather, it is possible to obtain a better fit to theoretical two terms linear approximation of Zoeppritz equation (Figure 45).

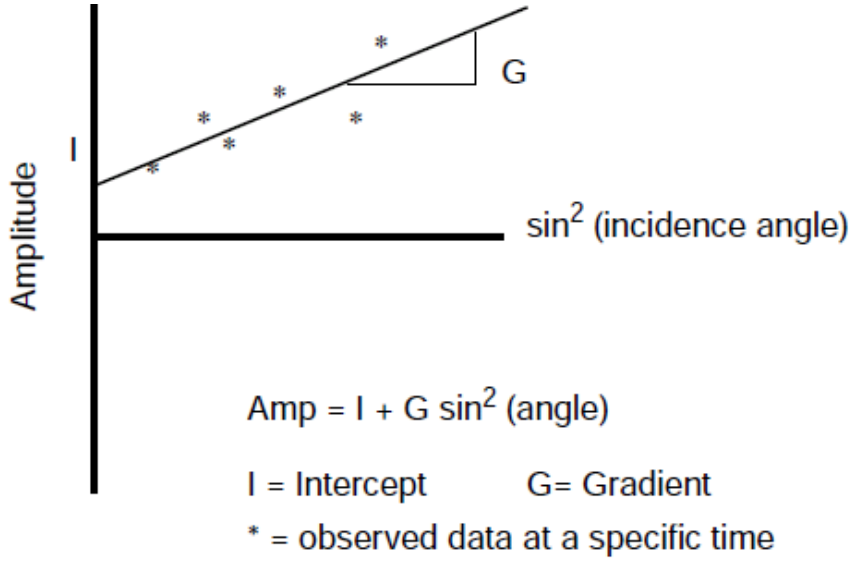

Figure 45. General squelch showing the concept of AVO Intercept and Gradient.

The slope line in Figure 45 is Shuey two terms linear approximation of Zoeppritz equation. Original two terms Shuey equation:

$$R(\theta) = R(0) + \mathrm{G}\sin^2\theta$$

Where: θ= Angle of Incidence; R= Reflection Coefficient; G =Gradient.

In real data acquisition it is impractical to have both shot and receiver in the same position. For this reason, real seismic data does not provide zero offset reflection information. However, this information can be calculated using theoretical equations such as Shuey's Equation. From the graphic in Figure 46, it can be seen that AVO intercept can be estimated by knowing the gradient amplitude, and extrapolating it to zero incidence angle axis. The slope line defined by Intercept, Gradient, and Angle of incidence is Shuey's two terms linear approximation of Zoeppritz equation.

Pad Intercept for Synthetic data

During Synthetic Study, synthetic data generated in Common Midpoint (CMP) domain had multiples, spike and random noise added (Figure 17). AVO intercept was estimated from this synthetic data in CMP domain with noise added, or input noisy gather. The first step is to generate angle limited CDP gather, which can be converted from NMO corrected CDP gather using Table Velocity. The converted angle gather had an angle range from 15 to 60 degree, the reason of choosing this angle range is to assure that the input gather is from mid and far offset, and it provided only the gradient information of the data. Afterward, the gradient amplitudes are used to estimate AVO intercepts (Figure 45 and 46).

Figure 46 shows seven intercept traces padded before the input noisy gathers. After AVO intercept trace was extracted from the input angle limited gathers, this trace was repeated seven times, and added in front of the original gather.

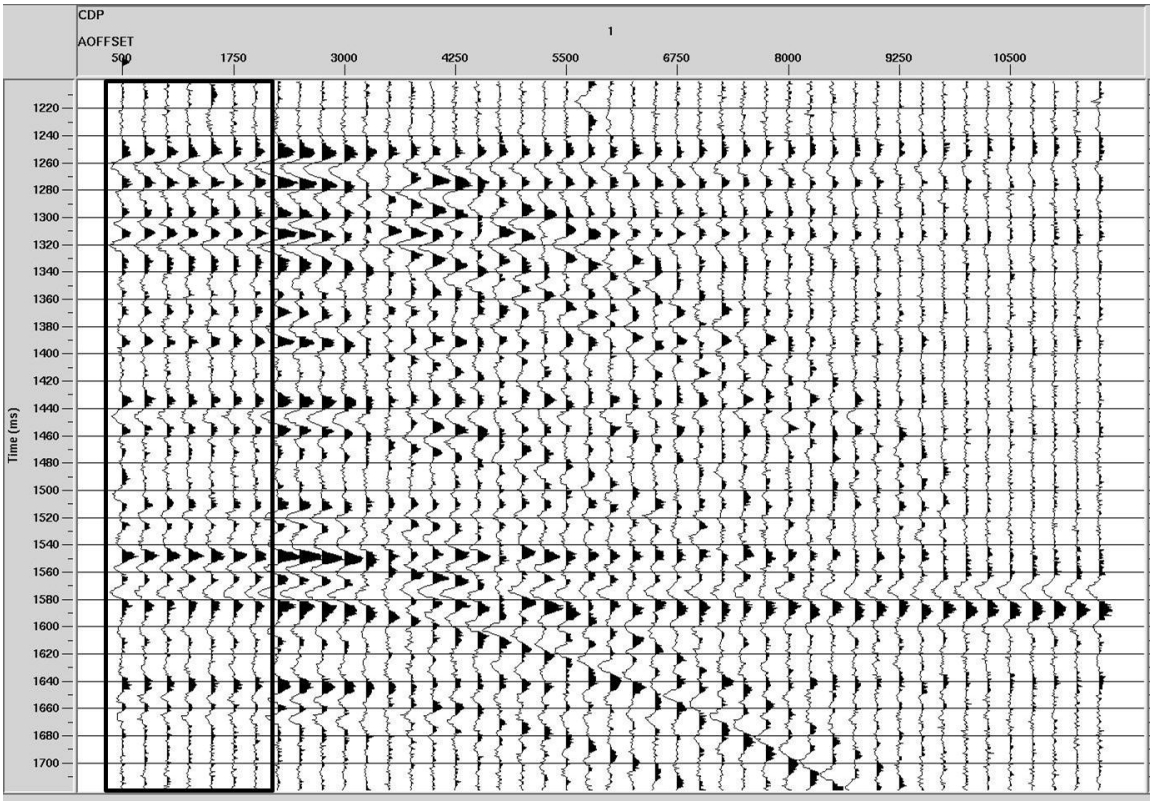

Figure 46. AVO Intercept padding for Synthetic noisy gather.

Pad Intercept for Real Data

While AVO intercept can be extracted from a single CDP gather in synthetic case, for real data the same method cannot be used. In real data application, the AVO intercept was added to the common offset filtered gather. Firstly the SF filtered common offset gathers was sorted them into CDP gather, then the CDP gathers was converted to angle limited gathers and extracted AVO intercept section. Afterward, the extracted intercept section was pad in front of the raw CRP gathers as offset 0 and 250 ft (0 and 75 m) before SF filtered common offset sections (the raw data had an offset range from 500 to 8000 ft or 150 to 2400 m). The final step is to sort common offset gathers back to CDP gathers and use these as input for pre-stack Structural Filter (flt20423).

Figure 47 shows two intercept traces padded before a single raw CRP gathers. After AVO intercept section was extracted from angle limited gathers, this was repeated twice and added in front of raw CRP gather sorted into common offset sections. When finished adding AVO intercept sections to common offset sections, the output volume can be resorted into CDP gathers. For purpose of illustration the CDP gather 8830 is presented.

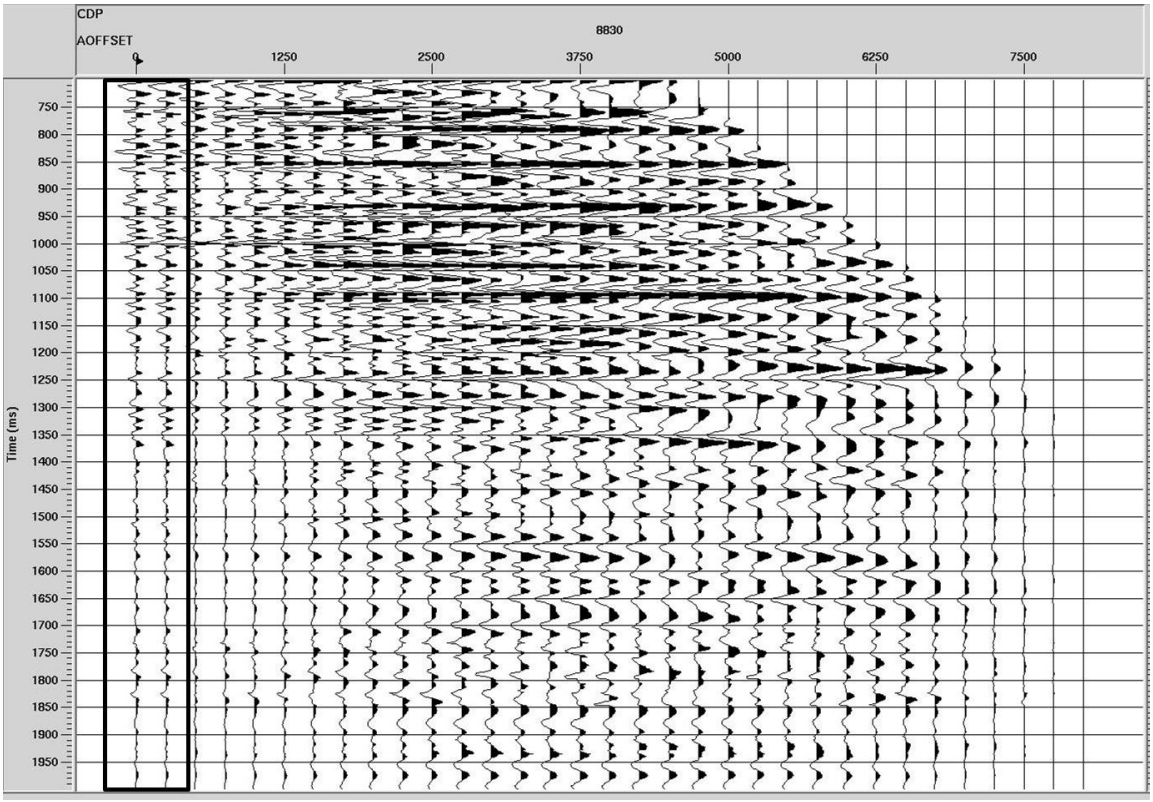

Figure 47. AVO Intercept padding for Raw CRP gather.

Appendix C

The Table Velocity is a theoretical velocity field that is given in time-velocity pair. It gives a reasonable approximation of the subsurface velocity field, by assuming that the layered medium is roughly homogeneous and isotropic.

In this thesis, the Table Velocity was used for AVO intercept extraction, and AVO gradient analysis in Synthetic Study; AVO intercept extraction, AVO intercept and gradient sections, and AVO intercept and gradient cross-plots in Real Data Application.

For all cases, the Table Velocity was mainly used to convert CDP gathers to Angle gather. The following table shows all velocity pairs within a Table Velocity:

Time (ms)	Velocity (ft/s)
0	4950
1500	4950
2000	6600
3000	9900
4000	13200
5000	16500
6000	19800

Table 1. Table Velocity showing all velocity pairs.